Spatiotemporal characteristics of current and projected rainfalls over East Africa: Insights from precipitation concentration and standardized precipitation indices

Abera Debebe Assamnew (aberradebebe@yahoo.com)
Addis Ababa University College of Natural Sciences https://orcid.org/0000-0003-2234-8086
Gizaw Mengistu Tsidu

Research Article

Keywords: HEM, RCP, GCM, CRU, rainfall, projection

Posted Date: May 9th, 2022

DOI: https://doi.org/10.21203/rs.3.rs-1433866/v1

Abstract

This study has used monthly rainfalls from Regional Climate Models (RCMs) experiments conducted in the frame work of the COrdinated Regional Downscaled EXperiment (CORDEX) project for historical and future periods. The deriving General Climate Models (GCMs) are obtained from Coupled Model Inter-comparison project phase 5 (CMIP5). Rainfalls from RCMs for the historical period, the two scenarios (i.e. Representative Concentration Pathway (RCP) scenarios representing radiative forcing of 4.5 m/W^2 (RCP4.5) and 8.5 m/W^2 (RCP8.5)) and Climate Research Unit (CRU) are used to determine precipitation concentration index (PCI), standardized precipitation index (SPI), and trend. The PCI, SPI, and trend derived from CRU and Historical Ensemble Mean (HEM) rainfalls are used to (1) assess the fidelity of the models in capturing observed spatiotemporal characteristics of rainfall over East Africa (EA) and (2) assess the relative change in the pattern of rainfall extremes and trends from the two scenario projections. From CRU and HEM-based SPI, the normal rainfall years are about 62–80% and 62–71% of the time of the historical period (1951–2005) during March-May (MAM) and September-December (SOND) respectively. The spatial dipole pattern captured by CRU and HEM is visible in the projections under the two scenarios implying that both radiative forcing are not expected to alter current rainfall regime over EA. In addition, normal rainfall is expected to occur for 62–68% and 65–72% of the time of the projection period (2006–2100) during MAM and SOND respectively. The projected rainfall shows wetting trend during MAM in contrast to the historical observations of dry trends over much of EA.

1. Introduction

There are ample direct and proxy observational evidences that global climate is changing on a wide range of time scales. However, the changes since pre-industrial times are attributed to anthropogenic activities according to various IPCC reports. In particular, the use of fossil fuels led to increase in carbon dioxide and other greenhouse gases in the atmosphere that altered the global energy balance (Allan & Soden, 2008). However, the observed climate changes in response to this energy imbalance are not uniform spatially across the globe. For example, Kenya, from East Africa (EA), experienced rise in temperature on average by about 0.21^{o} C per decade from the 1960s to 2006 (Hill, 1968). This rise in temperature over northern Kenya from October to February is coupled with a decrease in rainfall from long rains from March to May unlike that of southern Kenya (Stiebert et al., 2012). Consistent with this historical trend, climate projections for the northern Kenya have shown an increase in the incidence of drought, high temperature and water scarcity (Measham & Lumbasi, 2013; Muhati et al., 2018).

The spatial heterogeneity in climate change over EA is considerably high. The high rainfall variability and differences in trend over EA are attributed to the complex topography that allows varied local feedback to the radiative forcing (Yang et al., 2014; Omondi et al., 2014; Ntwali et al., 2016). In addition to the varied local response to climate change within EA, there are also changes in climate that are distinct and common to the whole region. For instance, the region receive mean total precipitation lower than the rest of the equatorial regions (Omondi et al., 2014). Moreover, the region regularly suffered from recurrent extreme weather conditions (Lyon & Dewitt, 2012; Liebmann et al., 2014) and has experienced

wetting/drying trends in short (long) rains respectively (Lyon & Dewitt, 2012; Yang et al., 2014; Bahaga et al., 2015). Most models have also suggested that there is an increase in temperature and rainfall over EA under various climate change scenarios in the 21s century (Williams & Funk, 2011; Jacob et al., 2012) under various climate change scenarios. However, the increase in projected rainfall under the various scenarios is inconsistent with what is observed over EA. Moreover, the underlying reason for this difference in rainfall trend over EA between projection and observations is not yet fully understood and referred to as the EA climate paradox (Wainwright et al., 2019) and references therein).

Despite the limitations in the skills of models, GCM simulations forced by specified variations in GHGs are commonly used to understand future climate change. For example, using ensemble of observations, reanalysis and simulations data set, (Wainwright et al., 2019) have indicated the rainfall decline in the historical period is, to some extent, related to a later onset and earlier cessation of the long rains. Therefore, there is a concerted effort to improve and use climate models. Coupled Model Intercomparison Project Phase 5 (CMIP5) (Taylor et al., 2011; Krishnan et al., 2019) is one of these international efforts. CMIP5 is driven by historical forcing for current climate and Representative Concentration Pathway (RCP) for projection under different scenarios (Allen et al., 2014). Each Pathway embedded a set of assumptions that lead to four levels of radiative forcing of 2.6, 4.5, 6.0, and 8.5 W /m^2, which is labeled as RCP2.6, RCP4.5, RCP6.0, and RCP8.5 respectively. The CMIP5 models are diverse in terms of model complexity, spatial and temporal resolutions. Yet, even the most complex and spatially highly resolved GCMs are not sufficient to resolve local scale processes. To overcome this limitation, dynamical downscaling of the GCMs to regional scale using RCM is preferred. As a result, Regional Climate Model (RCM) downscaling shows a considerable increase over the globe (Anyah & Semazzi, 2007) for simulations of both historical and projected scenarios. However, simulation of historical and projected scenarios using RCM is very few over EA (Brunswick et al., 2006; Segele et al., 2009; Diro et al., 2012). One of the few experiments is COordinated Regional Climate Downscaling EXperiment (CORDEX) which provides an opportunity of obtaining high-resolution RCM simulations for the historical and projection periods over the EA and the rest of the globe (Evans, 2011; Jacob et al., 2012; Gutowski et al., 2016). The CORDEX simulations of the historical ensemble and future climate as obtained from scenario projection have been used in the study of current and future climate variability and trend. Previous studies for example (Nguvava et al., 201; Mostafa et al., 2019) have employed CORDEX experiments to investigate current and projected climates under various scenarios over EA.

However, there is a significant model bias due to physical representation and parameterization in reproducing the observed rainfall which also varies from model to model and region to region over the globe (Allan & Soden, 2012; Kharin et al., 2007; Church et al., 2013). Various studies have been undertaken to assess the performance of models over EA. For example, (Yang et al., 2014) used five CMIP5 GCMs and identified that the outputs overestimate short rains and underestimate long rains. Models show weak performance in representing observed rainfall in the vicinity of the equator compared with the rest part of the region (Knutti & Sedlá˘, 2012; Woldemeskel et al., 2015. Ongoma et al., 2018; Ongoma et al., 2019) selected eight best performing GCMs from 22 CMIP5 coupled models over EA.

(Ayugi et al., 2019) used Rossby Center of Atmospheric Models (RCA4) driven by some CMIP5 GCMS in the simulation of precipitation over the Greater Horn of Africa (GHA) from 1951 to 2005. The authors identified MIROC5, CSIRO, CM5A-MR, Max Plank Institute for Technology (MPI-ESM-LR), and EC-EARTH as best performing GCMs in reproducing observed rainfall over EA. All selected models captured the bimodal and unimodal rainfalls distribution pattern. (Yisehak et al., 2021) studied spatiotemporal characteristics of meteorological drought under changing climate over the northern parts of Ethiopia using five CMIP5 GCMs namely CCSM4, GGFDL-ESM2M, HadGEM2-ES, MIROC5, and MPI-ESM-MR. The author identified that the projected rainfall shows an increasing trend over the northern parts of Ethiopia. Projected drought events are more frequent in RCP4.5 than in RCP8.5 projections (Yisehak et al., 2021). Recently, (Ngoma et al., 2021) used EC-EARTH, IPSL-CMA-MR, MIROC5, CSIRO-MK3.6.0 and MPI-ESM-LR downscaled with RCA4 to assess current and future spatiotemporal precipitation variability and trends over Uganda. The projected rainfall has wet condition between April/May and October whereas reduction in wet condition in March over Uganda (Ngoma et al., 2021). Ongoma et al., 2018) also used CanESM2, CESM1-CAM5, CNRM-CM5, CSIRO-MK3.6-0, and MIROC5 CMIP5 GCM to evaluate change in the mean rainfall projected under RCP4.5 and RCP8.5 over EA. Assamnew & Gizaw (2020) have also assessed CORDEX simulations and they have indicated that MPI, MIROC, CCCma, IPSL, CSIRO, MOHC and MIROC are best performing GCMs when coupled to RCA4 and REMO RCMs for downscaling in most of the rainy season over EA.

Motivated by the on-going improvements in the performance of models over the years, the data have also been used to investigate various aspects of climate change and its impact on water, agriculture, and health sectors. For example, (Gebrechorkos et al., 2018) used regional climate projections for impact assessment in EA. (Lyon & Dewitt, 2012) have shown the long rains over EA exhibits an increasing trend over western Ethiopia and Kenya in contrast to a decreasing trend over Tanzania. (Ongoma et al., 2018) evaluated change in mean rainfall and temperature over EA based on scenario projections from five CMIP5 models. The authors identified increase in rainfall under both RCP4.5 and RCP8.5. Moreover, they have indicated that the increase in rainfall from October to December exceeds that of March to May season. Similarly, (Ongoma et al., 2018) have noted the increase in projected rainfall under RCP8.5 exceeds that of RCP4.5.

The majority of these studies have focused on model validation, drought, decadal variability and long term change in rainfall over identified homogeneous rainfall regimes in EA. For example, (Ongoma et al., 2018) have evaluated changes in mean rainfall and temperature based on CMIP5 models using nine homogeneous sub regions over EA and evaluated decadal variability and trend of annual mean rainfalls. However, there is limited number of studies on precipitation extremes which increased in frequency of occurrence and intensified in recent decades. Precipitation extremes can be quantified by the frequency analysis of rainfall series and precipitation heterogeneity indexes. To our knowledge, we are not aware of any study that employ precipitation heterogeneity index to understand rainfall extremes in EA. In this study, precipitation concentration index (PCI), defined in terms of monthly rainfall series to quantify temporal distribution of precipitation within a given season or year is used to investigate spatiotemporal rainfall characteristics (Oliver, 1980; De Luis et al., 2011). PCI represents the degree to which monthly

precipitation is unevenly distributed throughout the season or year which then leads to rainfall extreme conditions such as drought. In addition, standardized precipitation index (SPI) is employed. Therefore, a comparative analysis of these extreme precipitation indices has scientific merit since they provide better understanding of recurrent and potential future drought events in the region. Moreover, the evaluation of rainfall trend and variability at each grid point allows identification of climate change hot spots which, to our knowledge, was not sufficiently covered in any of the previous studies. This is particularly important in view of complex topography that may not be captured by analysis over limited number of homogeneous rainfall regimes. Therefore, this study intends to address these problems and seeks answers to questions such as what is the skill of the mean of climate simulations for the historical period, hereafter referred to as historical Ensemble Mean (HEM), in capturing the observed seasonal precipitation heterogeneity over EA?; How projected rainfalls are changed relative to the HEM and observed (i.e. CRU) rainfalls over EA? In addition, comparison of rainfall trends from projections, observations and HEM during both short and long rains provides insight into a range of possible climate changes, and provides vital and appropriate information for the development of mitigation and adaptation options to climate change. The paper is organized such that Section 2 deals with methodology and Section 3 consists of results and discussion. Finally Section 4 presents conclusions.

2. Data And Methodology

2.1. Study area

EA, which is the area of this study, includes Ethiopia, Kenya, Somalia, South Sudan, Tanzania, eastern parts of DRC and Uganda. The region is complex in topography with different rainfall regimes. Identifying and conducting separate analysis for the major rainfall regime are necessary to come up with plausible results consistent with the dynamics of large scale atmospheric and oceanic circulations as well as with the local land and atmospheric feedbacks. Therefore, in addition to analysis at each grid point over EA, we have also taken three sub regions as defined in our previous study (Assamnew & Gizaw, 2020). The three sub regions for analysis of rainfall trend and variability are northern EA (NEA) located within: 5–15^{o} N, 27–47^{o} E), equatorial EA (EEA) located within: 5^{o} S – 5^{o} N, 27–47^{o} E), and southern EA (SEA) bounded by: 10–5^{o} S, 27–40^{o} E). NEA is characterized with boreal summer season from June to September as its main rainy season. March to May (MAM) is also considered as small rainy season over this sub region. EEA covers the equatorial parts of EA such as Somalia, Kenya, Uganda and northern parts of Tanzania. This region receives rain during March to May (MAM) and September to December (SOND). Finally, SEA represents southern parts of EA such as Tanzania and DRC and known with austral summer rainy season. The sub region receives its abundant rainfall from December to January (DJF) (see also Assamnew & Gizaw (2020)) for more details).

2.2. Data

Observed rainfall is taken from Climate Research Unit (CRU: version 4.04) of East Angela University (Mitchell & Jones, 2005). Model rainfalls are taken from CMIP5 repository, which is downscaled in the

framework of CORDEX. The models used for both HEM and scenario projections are selected by (Assamnew & Gizaw, 2020) (Assamnew & Gizaw, 2020) based on evaluation of their performance. CanESM2 is one of the selected models and it is a spectral model that employs triangular truncation with physics tendencies calculated on 128 X 64 points (~ 2.81^o) horizontal grid (Arora et al., 2011). The second generation Canadian Earth System Model (CanESM2) which is contributed by the Canadian Centre for Climate Modeling and Analysis (CCCma) has a resolution of T63 for atmosphere with a linear transform grid of 2.81^o, whereas the ocean component has horizontal grid spacing of 1.41^o in longitude and 0.94^o in latitude, and MPI-M uses T63 (1.875^o X 1.875^o) with triangular truncation (Giorgetta et al., 2013). The Commonwealth Scientific and Industrial Research Organization (CSIRO) and the Queensland Climate Change Center of Excellence (QCCCE) jointly contributed to CMIP5 using CSIRO-Mk3.6 model which depends on spectral model (T63) that utilizes the flux form of dynamical equations. The other models used in the study are Institute Pierre-Simon Laplace (IPSL), MIROC, and MPI-M. IPSL uses medium range resolution with 144 X 142 points (2.5^o X 1.25^o). MIROC has resolution of T85 (256 X 128) for atmosphere (Watanabe et al., 2010).

The two RCMs found to perform very well over EA when coupled to the above GCMs according to (Assamnew & Gizaw, 2020). are RCA4 (Samuelsson et al., 2011; Jones et al., 2011) and hydrostatic version of REgional MOdel (REMO). RCA4 has a different resolution and for this analysis, data with 0.44^o resolution is used (Wu et al., 2020). REMO is a hydrostatic regional climate model of three-dimensional atmospheric RCM developed at the Max Planck Institute of meteorology with a 0.44 o horizontal grid resolution (Elizalde et al., 2010). The rainfall projections used for this study are generated under RCP4.5 and RCP8.5 scenarios.

2.3. Methodology

In this study, long rains cover the period from March to May (MAM) and short rains includes months from September to December (SOND). Evaluation of anomalies for all rainfall data is based on a base period from 1971 to 2000. The statistical tools employed in this study are Sen’s slope estimator, SPI and PCI. We used the three parameters as defined below.

2.3.1. Sen’s slope estimator

When a given data has a trend, the magnitude can be determined using Sen’s slope estimator (Sen, 1968; Courtier et al., 2020). For n data points, the slope between Yi and Yj is given in Eq. 1 as

$$b_i = \frac{Y_j - Y_k}{j - k}$$

1

where Yj and Yk are the data value at time j and k (j > k) respectively. If there are N values of bi, then the N value of bi are ranked from smallest to largest from which the median of Sen’s slope estimator can be

computed as

$b_{med} = b_{\frac{N+1}{2}}$, if N is odd

$b_{med} = \frac{b_{\frac{N}{2}} + b_{\frac{N+2}{2}}}{2}$, if N is even

The statistical significance of the slope (i.e. trend) is evaluated using Eq. 2 as

$$t = \frac{b}{\frac{s_e}{\sqrt{(n-1)^2 s_x^2}}}$$

2

where b is slope and given by

$$b = r\frac{S_y}{S_x}$$

3

where r is correlation between variables x and y with sx and sy as standard deviation respectively. The standardized error of measurement se is defined as

$$s_e = S_y\sqrt{(1-r^2)}\sqrt{\frac{n-1}{n-2}}$$

4

2.3.2 Standardized Precipitation Index (SPI)

SPI is used to quantify precipitation deficit and can be evaluated using Eq. 5

$$SPI = \frac{p - P_I}{\sigma}$$

where P, Pi, and σ represent seasonal mean precipitation, seasonal precipitation and standard deviation respectively. SPI values categorized as > 2.0, 1.5 to 1.99, 1.0 to 1.49, 0.99 to − 0.99, -1.0 to -1.49, -1.5 to -1.99 and <-2.0 represent extremely wet, severely wet, moderately wet, near normal, moderately dry, severely dry, and extremely dry respectively (Bobadoye et al., 2016).

2.3.2. Precipitation Concentration Index (PCI)

PCI is a good indicator of temporal rainfall distribution in which a larger value indicates that rainfall is more concentrated within a subset of the whole duration (e.g., subset of a year or season) under

consideration (Oliver 1980; Luis et al 2011). The annual PCI at each grid point is given by Eq. 6:

$$PCI_{an} = \frac{\sum_1^{12} P_i^2}{\left(\sum_1^{12} P_i\right)^2} X100$$

6

Similarly, Eq. 6 is modified for seasonal PCI as in Eq. 7:

$$PCI_{sn} = \frac{\sum_1^{m} P_i^2}{\left(\sum_1^{m} P_i\right)^2} X\frac{100m}{12}$$

7

where m is the number of months for a specified season and Pi is monthly rainfall in month i of a given season.

The lowest possible value of PCI is 8.3 which indicate all months within a year or a season contribute to the total rainfalls equally. In general, small value of PCI shows uniform distribution among the component months of the season or a year. According to Oliver (1980), PCI ≤ 10 is considered as a range of PC that describes uniform temporal distribution. Moderately uniform, irregular and strongly irregular temporal rainfall distributions are given by the following PC ranges: 10 < PCI ≤ 15, 15 < PCI ≤ 20 and PCI > 20) respectively. To appreciate the significance of these categories, it is important to look at some specific figures from these ranges. A PCI value of 16.7 indicates that the total rainfall is concentrated in half of the period whereas a PCI value of 25 indicates that rainfall occurred in one-third of the period. In other words, annual PCI value of 25 indicates that the total rainfall occurred in only four months of a year whereas for a season of three months, this figure implies the rainfall occurred in just one month.

3. Results And Discussion

3.1. Rainfall variability and trend during the historical period (1951–2005)

3.1.1. Climatology of CRU and HEM rainfalls

The seasonal climatology of short and long rains derived from CRU, HEM and scenario projections over EA are given in Fig. 1. The temporal mean shows that CRU and HEM have similar spatial pattern as reflected in the presence of the dipole rainfall pattern during both MAM and SOND seasons (Fig. 1). The spatial dipole rainfall patterns during the two seasons were also captured from observations and reported by previous studies (Ongoma et al., 2018). As noted also in the previous studies (Ongoma et al., 2018),

the spatial dipole pattern in the mean seasonal rainfall is not symmetric since the mean rainfall at one side of the dipole far exceeds the other end of the dipole. Therefore, the side of the dipole with maximum rainfall is referred to as main peak and the other end of the dipole is referred to as minor peak.

The main peak of the spatial dipole pattern observed in long rains (Fig. 1a-b) is located over the southwestern part of EA (i.e. Uganda, Kenya, northern Tanzania, and DRC) and the minor peak over the western Ethiopian highlands. The mean climatology of CRU rainfalls during MAM shows that region from South Sudan to Kenya through the Turkana lowland, northern Uganda, Kenya, Somalia, southeastern, eastern and northern parts of Ethiopia are dry. However, the areas under the same dry condition based on HEM climatology are broader than that of CRU (Fig. 1a). CRU rainfall distributions over South Sudan and Ethiopia are not well represented by HEM. HEM shows higher rainfall than CRU over DRC. HEM has underestimated CRU over most parts of EA such as eastern DRC, southern and central Ethiopia, Tanzania, western Kenya, and Uganda (Fig. 1a-b) during MAM in agreement with previous studies (Yang et al., 2015; Ongoma et al., 2019; Ayugi et al., 2019).

The long term mean of seasonal rainfall spatial pattern for short rains (SOND) over EA is depicted in Fig. 1 (c-d) for the historical period. The dipole spatial pattern of mean CRU rainfalls during short rains can be characterized as having the main peak over Uganda, Kenya, Tanzania and DRC, and the minor peak over western Ethiopia (Fig. 1c). HEM has reproduced the climatological spatial rainfall distribution of CRU over DRC and the adjoining parts of Tanzania in contrast to the climatology over western parts of Ethiopia (Fig. 1d). Tanzania has more coverage of wet areas according to HEM than CRU. Moreover, HEM has higher rainfall than CRU over DRC and adjoining areas in Uganda and Tanzania. Apart from this, HEM has a wet bias over eastern DRC, small areas over south central Ethiopia, southwestern Kenya and Tanzania. This wet bias is also reported by the previous studies (Yang et al., 2015; Ayugi et al., 2019). In contrast, HEM has dry bias relative to CRU rainfalls over DRC, central and western Ethiopia (Fig. 1b, d).

3.1.2. CRU and HEM seasonal rainfalls trends

The rainfall trends for the three homogeneous rainfall regimes and the whole EA are determined from spatially averaged MAM and SOND rainfalls (Table 1). In addition to the regional rainfall trends, Fig. 2a shows rainfall trends at each grid point determined from CRU and HEM rainfalls. Seasonal rainfall trends over the period from 1951 to 2005 are calculated using Sen's slope estimator (see Eqs. 1 to 4). Dry trends are exhibited by CRU MAM rainfall over EEA, SEA and the whole EA whereas dry trends are estimated from HEM MAM rainfall over NEA, SEA and the whole EA. Similarly, dry trends are determined from CRU rainfall during SOND over NEA and SEA and HEM over SEA. On the other hand, CRU rainfalls over NEA and HEM rainfalls over EEA show wet trends during MAM. CRU over EEA and the whole EA as well as HEM over NEA, EEA and the whole EA has a wet trend during SOND (Table 1). These wet trends observed in CRU and HEM rainfalls during SOND are in agreement with findings of (Bahaga et al., 2015). The magnitude of rainfall trends determined from CRU and HEM rainfalls are different over all regions and in both seasons (Table 1). This marked difference is likely due to bias in the models used for the ensemble mean since there was no any bias correction applied to CORDEX simulations from which HEM is determined. However, HEM and CRU rainfalls have the same direction of trend over SEA (-) and the whole

EA (-) during MAM and over EEA (+), SEA (-) and the whole EA (-) during SOND. The leading dry trend is -2.42 mm/decade over SEA as seen in CRU and − 0.85 mm/decade over SEA from HEM during MAM and − 0.47 mm/decade over SEA from CRU and − 0.29 mm/decade over SEA from HEM rainfall during SOND. The leading dry trend is observed over SEA during both seasons. CRU and HEM rainfalls have opposite trend over NEA in which HEM has negative during MAM and positive during SOND. HEM rainfall has shown more of wet trend than CRU during both seasons. This dry trend particularly during long rains is also in line with previous studies (Lyon & Dewitt, 2012; Liebmann et al., 2014; Yang et al., 2014; Nicholson, 2017) which showed the decreasing trend from the 1980s onwards. HEM has shown a stepper wetting trend over EEA than over NEA and SEA during MAM (See Table 1).

Table 1
Spatial mean trend of long and short rains over each sub region from 1951 to 2005 for CRU and HEM rainfalls (mm/decade).

Sub region	MAM		SOND	
	CRU	GPCC	CRU	GPCC
NEA	0.44	-0.37	-0.38	0.89
EEA	-2.35	0.18	0.29	0.92
SEA	-2.42	-0.85	-0.47	-0.29
EA	-1.11	-0.08	0.04	0.83

CRU MAM rainfall has drying trends over the whole parts of EA except central and northeastern Ethiopia, some areas in Sudan Republic and eastern Somalia (Fig. 2). The areas with wet trend as determined from HEM MAM rainfalls include small areas in the eastern part of EA that extend from southeast to northeast part of Ethiopia, central and northern Kenya, and DRC and isolated places in Uganda (Fig. 2c). Therefore, there are notable difference between trends estimated from CRU and HEM over northern EA and equatorial EA. CRU reveals wetting trends over northern EA (Fig. 2a) in contrast to HEM (Fig. 2c); and CRU reveals drying trend over equatorial EA as opposed to wetting trend of HEM rainfall. Although the area under wetting trend of CRU rainfall and drying trend of HEM does not cover the whole area designated as NEA in Section 2.1, the CRU and HEM rainfall trends determined from NEA regional mean rainfalls are consistent with trends at each grid point (Table 1). The dry trends from CRU MAM rainfalls over most parts of EA are in agreement with the previous studies (Lyon & Dewitt, 2012; Williams & Funk, 2011; Yang et al., 2014). On the other hand, CRU SOND rainfalls over northwestern Ethiopia and the adjoining areas in South Sudan, central and western areas in Kenya, central and eastern areas in Tanzania, and western parts of DRC were decreasing during the last 55 years. In contrast, HEM simulations could not capture these drying trends, specifically over Ethiopia, Kenya and South Sudan (Fig. 2b, d). While these are the notable differences, there are also agreements at least in the direction of change of rainfall between CRU and HEM rainfalls. For instance, HEM rainfall has shown wetting trend over isolated places in Ethiopia, Kenya and Uganda where CRU also exhibits wetting trend, which is less than 0.5 mm/decade,(Fig. 2b, d).

The increasing tendency of short rains over EA particularly over EEA is in agreement with a number of research results (e.g. (Liebmann et al., 2014; Nicholson, 2017). Although trends calculated from regional mean rainfall is sensitive to the area included in the averaging and the length of the time series, several authors identified increasing SOND rainfall in the region for the last few decades. For example, (Cattani et al., 2018) has identified increasing trends for the October-November-December and decreasing trends in MAM rainfalls over East Africa (5^{o} S-20^{o} N, 28-52^{o} E) from 1983 to 2015 from Climate Prediction Center (CPC) Africa Rainfall Climatology version 2.0 (ARC2), Climate Hazards Group InfraRed Precipitation with Stations (CHIRPS) and Tropical Applications of Meteorology using SATellite (TAMSAT) African Rainfall Climatology And Time series version 2 (TARCAT) rainfall datasets.

3.1.3. Spatiotemporal variability of rainfall extremes from CRU and HEM SPI

The variability of rainfall extreme during long and short rains over EA is investigated in this section using SPI derived from CRU and HEM rainfalls. The CRU and HEM SPI (Table 2) have both dry and wet trends over parts of EA and the whole EA. In a few cases, the two-SPI time series (i.e. CRU and HEM SPIs) exhibit either opposing or considerably different magnitude of linear trends (Table 2). The CRU and HEM SPI trends are consistent with trends derived from the rainfalls. As a result, the sign of trend of SPI (normalized time series of CRU and HEM rainfalls) (see Table 2) is same as sign of trend estimated from rainfall time series using Sen's slope estimator (see Table 1).

Table 2
Trend of CRU and HEM SPIs from 1951 to 2005 per decade.

Sub region	MAM		SOND	
	CRU	GPCC	CRU	GPCC
NEA	0.06	-0.05	-0.06	0.14
EEA	-0.18	0.01	0.02	0.07
SEA	-0.16	-0.06	-0.02	-0.02
EA	-0.15	-0.01	0.01	0.09

The percentage frequency of occurrence of extreme and normal rainfalls based on SPI classification for CRU and HEM rainfalls over EA and its three sub regions are given in Fig. 3. Figure 3 shows that near-normal rainfall accounts for approximately 64% − 71% of CRU and 62% − 80% of HEM rainfalls during MAM and 62% − 71% of CRU and 65% − 71% of HEM rainfalls during SOND over the whole region and sub regions over the period from 1951 to 2005. This indicates that the study period has moderate to extremely wet (SPI > 1) and moderate to extremely dry (SPI<-1) conditions that occurred in 20% − 38% of the time from 1951 to 2005 (i.e., approximately 11–21 years of the 55 years period). HEM MAM rainfall is characterized by more of dry SPI (12.7%) than wet SPI (7.3%) over NEA. In comparison, CRU MAM rainfall has wet (12.7%) and dries (18.2%) conditions over EEA. Wet (dry) SPI from HEM over NEA, EEA, and SEA

are 7.3% (12.7%), 16.4% (14.6%) and 20.0% (18.2%) respectively. Similarly SPI from CRU over NEA, EEA and SEA are 16.4% (12.7%), 12.7%(18.2%) and 16.4% (14.6%) respectively (Fig. 3a). The number of wet SPI events captured by HEM rainfall over NEA and SEA is greater than dry SPI events.

Similarly, during short rain (SOND), normal rainfall (SPI from 1 to -1) accounts for about 62% – 71% of CRU and 65% – 71% of HEM rainfall events. The number of wet events over NEA and SEA is more than the number of dry events of HEM rainfalls. Wet (dry) conditions over NEA, EEA and SEA occurred 20.0% (14.5%), 16.4% (16.4%) and 16.4% (12.7%) of the time of regionally averaged HEM rainfall respectively. Similarly, regionally averaged CRU rainfall accounts for 18.2% (20.0%), 20.0% (14.5%) and 16.4% (12.7%) wet (dry) events over NEA, EEA and SEA respectively (Fig. 3). CRU and HEM have more wet than dry events over SEA. In general, the proportion of wet and dry events from SPIs calculated from regionally averaged HEM and CRU rainfalls is consistent with the wetting trends during SOND and the wet bias identified in HEM during MAM seasons in Sections 3.1.1–3.1.2.

The percentage of seasonal wet (SPI $\geq$ 1) and dry (SPI $\leq$ -1) events at each grid point from 1951 to 2005 is given in Fig. 4. The fraction of wet events captured by CRU and HEM SPIs (Fig. 4a-b) is comparable at most places over EA during MAM in contrast to a significant difference during SOND (Fig. 4c-d). On the other hand, the fractions of dry events captured by CRU and HEM rainfalls during MAM and SOND over EA exhibit substantial differences (Fig. 4e-h). It is also important to compare the difference between percentage of wet events and dry events as captured by both CRU and HEM rainfalls during the historical period for the two rainy seasons. The difference between the percentage of wet events and dry events over EA is shown in Fig. 4i-l. Figure 4i-j (red shaded map color) shows that most EA has experienced more dry events than wet events during MAM as captured by both CRU and HEM. However, there are a few isolated places dominated by wet events according to CRU rainfalls (blue shaded map color) as compared to dry events. Relative to CRU SPI, significant number of grids over EEA and SEA have witnessed more of wet than dry events based on SPI from HEM rainfalls (Fig. 4j). During SOND, CRU rainfall shows wet events that are more frequent than dry events over nearly half of the areas in EA (Fig. 4k). In contrast, the frequency of wet and dry events in HEM rainfalls during SOND is comparable over most parts of EA (Fig. 4l) revealing HEM rainfalls did not capture the observed distribution of extreme rainfalls as depicted in CRU (Fig. 4k). The overall mean percentage has indicated that 15.5% (15.8%) from CRU (Fig. 4a, e) and 16.4% (16.1%) from HEM (Fig. 4b, f) during MAM, and 16.1% (15.1%) from CRU (Fig. 4c, g) and 16.4% (15.8%) from HEM (Fig. 4d, h) during SOND are wet (dry) events respectively. The average normal events of CRU (HEM) are 68.7% (67.5%) during MAM and 68.8% (67.8%) during SOND respectively. The overall feature over EA with respect to wet and dry proportions of CRU and HEM rainfalls, it can be concluded that wet events are more numerous than dry events in HEM rainfalls during MAM and SOND whereas this is true for CRU rainfall during SOND. However, (Wang et al., 2017) using CRU from 1901 to 2010 over EA (40.75^{o} E – 51.75^{o} E longitude and 2^{o} S – 12.25^{o} N latitude) identified that OND revealed more drought instances as compared to MAM but the frequency of occurrence of moderate, severe, and extreme dryness was almost the same in both seasons. The minor

difference between their findings and the current analysis may be due to difference in domain size and length of the season.

3.1.4. Spatiotemporal variability of HEM and CRU PCI

PCI derived from regional mean of CRU and HEM rainfalls over each sub region is given in Table 3. The CRU and HEM PCI values over EEA clearly show that CRU and HEM rainfalls are uniformly distributed among component months of the seasons. For example, HEM PCI over EEA and the whole EA shows that the temporal rainfall distribution within MAM is 100% uniform throughout the 1951–2005 period. Unlike EEA, the temporal distribution of CRU rainfall within MAM over NEA is moderate (50.9%) and uniform (49.1%) throughout the study period (see Table 3). Similarly, CRU PCI reveals presence of uniform (27.3%) and moderate (72.7%) temporal distribution of rainfall within MAM season over SEA. The temporal distribution of rainfalls from CRU and HEM within both MAM and SOND over the region as whole is uniformly and moderately distributed. HEM PCI has shown moderate (72.7%) and irregular (27.3%) over NEA, uniform (98.2%) over EEA, and moderate (100%) distribution within MAM over SEA. Likewise, the PCI of HEM and CRU rainfalls over each subregion during boreal autumn season show uniform distribution within months. CRU has more of moderate (90.9%) and uniform (9.1%) PCI over NEA, uniform (100%) PCI over EEA, and moderate (100%) PCI over SEA respectively. Similarly, HEM has moderate (83.6%) PCI over NEA, uniform (100%) PCI over EEA, and moderate (100%) over SEA within SOND. NEA is the region with different categories of temporal rainfall distribution within MAM and SOND seasons according to both CRU and HEM data sets (Table 3).

Table 3
Number of years with uniform, moderate, irregular and strong irregular PCI values in MAM and SOND from 1951 to 2005

Rainfall	PCI range	MAM				SOND			
		NEA	EEA	SEA	EA	NEA	EEA	SEA	EA
CRU	$8.3 < PCI \leq 10$	27	55	15	55	5	55	0	55
	$10 < PCI \leq 15$	28	0	40	0	50	0	55	0
	$15 < PCI \leq 20$	0	0	0	0	0	0	0	0
GPCC	$8.3 < PCI \leq 10$	0	54	0	55	0	55	0	55
	$10 < PCI \leq 15$	40	1	55	0	46	0	55	0
	$15 < PCI \leq 20$	15	0	0	0	9	0	0	0

Apart from the frequency of the different categories of temporal rainfall distribution shown in Table 3, the shift from one category to another can be captured by investigating the trend in PCI. These trends over the different sub regions of EA and the whole EA derived from PCI based on CRU and HEM are given in Table 4. CRU and HEM PCI (Table 4) have mixed sign of linear trends over all parts of EA. MAM PCI from CRU over EEA and the whole EA and from HEM over NEA have a trend that shows decrease in PCI with

time. In contrast, PCIs from CRU over NEA and SEA from HEM over EEA, SEA and the whole EA have upward trend that shows change in the direction from moderate to more of irregular PCI with time. Trend over the whole EA is downward (upward) for CRU (HEM) rainfalls suggesting that observed rainfall concentration (CRU) within MAM season has exhibited a shift towards more uniform rainfall distribution within the three months with time in contrast to HEM that has exhibited more heterogeneity with time (Table 3). On the other hand, during SOND, CRU-based PCI over NEA and SEA, and HEM-based PCI over NEA have decreasing trends. In the same season, PCI trends obtained from CRU over EEA and from HEM over EEA, SEA and the whole EA show increasing heterogeneity. However, on regional basis, most of the trends are not large enough to change the categories of PCI over the period of study. PCIs from CRU and HEM have the same sign of trend over SEA (+) during MAM and over NEA (-) and EEA (+) during SOND (Table 4).

Table 4
PCI trend of CRU and HEM rainfalls from 1951 to 2005 per decade.

Sub region	MAM		SOND	
	CRU	GPCC	CRU	GPCC
NEA	0.05	-0.07	-0.05	-0.22
EEA	-0.02	0.04	0.01	0.03
SEA	0.04	0.09	-0.16	0.08
EA	-0.02	0.01	-0.02	0.01

The long-term mean of PCI derived from HEM and CRU rainfalls over EA during MAM and SOND are given in Fig. 5. Rainfalls from both HEM and CRU are uniformly and moderately distributed within the three months of MAM. CRU-based PCI over Ethiopia (covering areas that extend from southwest to northeast), DRC, Uganda, most parts of Kenya, and adjoining parts of Tanzania (mostly between 5^{o} S to 5^{o} N) is in the range of uniform distribution. The rest of EA covering southern Tanzania, southern DRC, eastern and northwestern Ethiopia, eastern Kenya, northern South Sudan, south of the Sudan Republic, and Somalia have temporal rainfall distributions that are in the range of moderate PCI. HEM-based PCI is mainly in the range of uniform temporal distribution over central DRC, Uganda, northern Tanzania, Kenya and northeastern Ethiopia. The rest of EA is covered with moderate PCI values but around the upper limit (i.e., PCI = 14 over southern Tanzania). Areal coverage of CRU-based uniform PCI is more than that of HEM-based uniform PCI. There is no PCI value in the category of irregular distribution during MAM from both CRU (except small area over Sudan Republic) and HEM (Fig. 5a-b). Similarly, grid point CRU PCI shows that temporal rainfall distribution during SOND is uniform over central and eastern DRC, southwestern Ethiopia, Uganda and the adjoining parts of Tanzania, Kenya and South Sudan. HEM rainfall has also uniform PCI over central and eastern DRC, southern Uganda, northern Tanzania and some areas over northwestern Kenya and northeastern Ethiopia. Sudan Republic, northern Ethiopia and central and southwestern Tanzania have temporal rainfall distribution that can be characterized as irregular whereas

Sudan Republic, northwestern Ethiopia and southern Ethiopia are found to have irregular rainfall within SOND season (Fig. 5c-d). The proportion of the areal coverage of PCI categories is dominated by moderate rainfall distribution within both long and short seasons. Uniform concentration of rainfalls follows the uniform rainfall distribution in terms of proportion of the area covered. Irregular and strongly irregular temporal rainfall distributions are also visible over some areas in EA.

3.2. Climatology, variability and trend of projected rainfalls under RCP4.5 and RCP8.5 scenarios

We have already identified CanESM2, CSIRO, MIROC, MPI and IPSL as the best GCM-RCM combination (Assamnew & Gizaw, 2020) in reproducing observed rainfall over EA. The simulations for the historical period referred to as HEM in this study (see Section 3.1) are based on these models. The projections from same models are used to produce ensemble mean projections under RCP4.5 and RCP8.5 scenarios. The same models are used for the analysis of projected scenarios. The annual cycles of projected rainfall, HEM, and CRU are given in Fig. 6. HEM and CRU are included in Fig. 6 to determine how the seasonality in rainfall varies during projections as compared to observations and model simulations during the historical period. Observed mean value of annual cycle from CRU rainfall is well captured by the HEM annual cycle with the exception of a minor difference in the magnitude of the long term mean monthly rainfall during some months. Moreover, the regional mean annual cycle of rainfall over all parts of EA and the whole EA during the projection period under the two scenarios remain the same as the cycles observed in the CRU and HEM rainfalls during the historical period (Fig. 6). This implies the phase of the annual cycles of rainfall over EA will not change under optimal RCP 4.5 and business as usual RCP8.5 scenarios. However, there are also notable differences between the observed seasonal rainfalls from June to September with the maximum difference observed in July over NEA; from October to December and March to May over EEA with a peak difference noted in November; and from November to February over SEA with a peak difference also noted in November. Spatial mean over the whole EA has shown that rainfalls will increase under both projected scenarios during October and November. The highest mean values from July to September over NEA, March to May and October to November over EEA and November to April over SEA under projected scenarios are in line with the observed rainfall climatology of the regions. Spatial mean of projected rainfalls over the whole EA are of the same range as simulated HEM rainfall. In contrast, spatial mean of CRU rainfall exhibits appreciable difference from both HEM and projections. This may suggest that the common factor that influences both HEM and projected ensemble mean rainfall is the bias in the model. Such a relation between RCP4.5 and RCP8.5 are also identified by (Lyon & Vigaud, 2017; Muhati et al., 2018; Ongoma et al., 2018). Muhati et al., 2018) has also confirmed that projections under RCP8.5 are wetter than projections under RCP4.5 during OND.

3.2.1. Climatology of projected rainfalls

Since the spatial pattern of the mean MAM rainfall climatology under the RCP4.5 and RCP8.5 scenarios are fairly similar to that of HEM climatology, the differences between CRU and HEM that have been described so far can also be considered as the differences between observations (CRU) and rainfall

projections. The spatial pattern of projected rainfalls under the two scenarios is depicted in Fig. 7. As captured well in the HEM and CRU rainfalls (see Fig. 1), the north-south seasonal movement of ITCZ (i.e. northward during long rains and southward during short rains) are also well represented under both RCPs scenarios. Rainfall projections under both scenarios led to similar spatial rainfall distribution as that of the historical period during MAM. As a result, Uganda and adjoining parts of DRC, Kenya and coast of Tanzania are expected to have the highest rainfall relative to the rest of EA. There will also be areas over central parts of Ethiopia with the highest projected rainfall as compared to the neighboring countries. In contrast, Turkana lowlands extending from Kenya to South Sudan, South Sudan and northern and eastern parts of Ethiopia will remain dry. Eastern and central Ethiopia, Uganda and DRC are also expected to be wetter under RCP8.5 than under RCP4.5 projection. (Ongoma et al., 2018) showed spatial mean value that shows a clear difference between RCP8.5 and RCP4.5 using a domain between 12^{o} S – 5^{o} N and 28^{o} E – 42^{o} E.

Similarly, SOND rainfall (Fig. 7c-d), derived from the ensemble mean of projections from the two RCMs driven by the five GCM models, has exhibited similar mean distribution as during MAM (Fig. 7a-b). The highest ensemble mean rainfall is expected over Uganda and adjoining parts of Kenya, South Sudan, DRC, and adjoining parts of Tanzania under both scenarios. Areas extending from central Kenya to South Sudan through Turkana lowlands, South Sudan, eastern and southeastern parts of Ethiopia are expected to remain dry under the two scenarios. RCP8.5 is anticipated to be wetter than RCP4.5 over most parts of EA particularly over Somalia, southeastern Ethiopia and coast of Kenya which is in agreement with previous studies (Muhati et al., 2018; Ongoma et al., 2018) using partly different models.

3.2.2. Trend of projected rainfalls

Trends of regional mean of rainfalls projected under RCP4.5 and RCP8.5 during boreal spring and autumn seasons are given in Table 5. Regional mean rainfall exhibits wetting trend under RCP4.5 scenarios over EEA, SEA and the whole EA during MAM (Table 5). Similarly, the regional mean rainfall from RCP8.5 scenarios shows wet trend over EEA, SEA and the whole EA during MAM. Moreover, trends under both RCP4.5 and RCP8.5 are positive over EEA, SEA and whole EA during MAM. On the contrary, rainfall trend under both projected scenarios is expected to be relatively dry over NEA. The trends of regional mean rainfalls under RCP4.5 (RCP8.5) are estimated to be 0.92 (0.65) mm/decade over EEA (SEA) respectively. During SOND, regional mean rainfall obtained under RCP4.5 scenario has dry trend over SEA. Similarly, projected regional mean rainfalls under RCP8.5 have wet trends over all sub regions. The maximum wet trends from all the regions under RCP4.5 (RCP8.5) are 0.72 (2.11) mm/decade over EEA (EEA) respectively. During SOND, regional mean rainfall obtained under RCP4.5 scenario has dry trend over SEA. Similarly, projected regional mean rainfalls under RCP8.5 have wet trends over all sub regions. The maximum wet trends from all the regions under RCP4.5 (RCP8.5) are 0.72 (2.11) mm/decade over EEA (EEA) respectively. Trends from RCP4.5 and RCP8.5 have same sign over NEA (-), EEA (+), SEA (-) and EA (+) during MAM and NEA (+), EEA (+) and EA (+) during SOND. Moreover, both RCPs have wet trends over EEA (+) and the whole EA (+) during both seasons. Projected rainfall trends

under RCP4.5 and RCP8.5 have opposite sign over SEA (-) during SOND. The regional mean rainfall trend under RCP8.5 is wet over EA and its sub regions during SOND.

Table 5
Spatial mean trend (mm/decades) over each sub region in MAM and SOND from 2021 to 2080 for both projected scenarios.

Sub region	MAM		SOND	
	RCP4.5	RCP8.5	RCP4.5	RCP8.5
NEA	-0.32	-0.06	0.45	1.20
EEA	0.92	0.51	0.72	2.11
SEA	0.21	0.65	-1.59	0.14
EA	0.28	0.32	0.23	1.39

The projected rainfall trend at each grid point over EA under RCP4.5 and RCP8.5 scenarios is given in Fig. 8. The majority areas of the region are under dry trend particularly under RCP4.5. The southern and southeastern parts of Ethiopia, Kenya and adjoining parts of Uganda and Somalia have weak trend under RCP4.5 and RCP8.5. Areas over southeastern Ethiopia and northern Kenya under RCP4.5 and isolated areas over southeastern Ethiopia under RP8.5 have wet trend. The western parts of EA over DRC, South Sudan, Tanzania and western Uganda have strong dry trend (about 4 mm/decade) under both scenarios. The eastern parts of EA covering eastern coast of Tanzania, Kenya, Somalia, and southeastern Ethiopia have weak trend (Fig. 8a, c). During SOND, projected rainfall under RCP4.5 has shown wet trend over Ethiopia, Kenya and Somalia (Fig. 8b). Projected rainfall under RCP8.5 also shows wet trend over Sudan Republic, South Sudan, the whole Ethiopia, northern Tanzania, northern DRC, Somalia, Kenya and Uganda (Fig. 8d). In terms of areas covered under RCP8.5 cover more areas in EA than wet trend under RCP4.5 during SOND. These imply that the eastern part of EA along the coastal part of Indian Ocean is expected to receive high rainfall under both scenarios during both seasons. SOND is getting wetter than MAM under RCP8.5 over the course of the projection period (Fig. 8d). As a whole, projected rainfall over Kenya, Somalia, Uganda and Ethiopia show wet trend whereas rainfalls over DRC and adjoining parts of Tanzania show dry trend under both scenarios during the two seasons (Fig. 8). In addition, projected rainfalls under the two scenarios show dry trend over northern and northwestern part of Ethiopia, South Sudan, Sudan Republic, Uganda, DRC and Tanzania which is similar to that of observed CRU rainfalls during MAM. This similarity between trends of projected and observed rainfalls is also noted over DRC and adjoining parts of Tanzania during SOND. Projected rainfalls under both scenarios and observed CRU rainfalls have trends of opposite sign during MAM particularly over the eastern coast of EA such as Kenya, Somalia and southeastern parts of Ethiopia (See Fig. 2a and Fig. 8a-c). This wetting trend in the models during projection in contrast to drying trend in the current climate is long known as the East Africa paradox which is not yet resolved in the CORDEX experiments (Lyon & Vigaud, 2017; Wainwright et al., 2019). Recently, (Wainwright et al., 2019) suggested that the cause of the difference is related to the

change in the onset and cessation of the seasons in the historical rainfalls. Finally, it is also interesting to note that RCP8.5 is wetter than RCP4.5 during SOND.

3.2.3. Spatiotemporal variability of projected SPI

Trends of SPI determined from projected rainfalls under RCP4.5 and RCP8.5 scenarios for both short and long rains are given in Table 6. The linear trend of SPI is positive over EEA, SEA, and the whole EA under RCP4.5 during MAM. The SPI trend is also positive over EEA, SEA and the whole EA under RCP8.5 in the same season (Table 6). Similarly, SPI trends over NEA, EEA and the whole EA under RCP4.5 and over all sub regions under RCP8.5 are positive during SOND. SPI derived from projected rainfalls under RCP4.5 and RCP8.5 scenarios have trends with the same sign over NEA (-), EEA (+), SEA (+) and the whole EA (+) during MAM, and over NEA (+), EEA (+) and the whole EA (-) during SOND (Table 6). Since SPI is a normalized time series of rainfall, the SPI trends are expected to point in the same direction as that of the rainfall itself as indicated in Table 5.

Table 6
Trend of SPI from rainfalls projected under RCP4.5 and RCP8.5 from 2021 to 2080 per decade.

Sub region	MAM		SOND	
	RCP4.5	RCP8.5	RCP4.5	RCP8.5
NEA	-0.09	-0.02	0.17	0.32
EEA	0.15	0.08	0.15	0.32
SEA	0.03	0.09	-0.22	0.02
EA	0.08	0.09	0.07	0.31

The percentage of normal rainfall years within each region under both scenarios accounts for more than 68% (RCP8.5) and 62% (RCP4.5) of the whole duration (2021–2080). The normal years based on rainfall condition in each season is defined as having SPI values from − 1 to 1. Figure 9a for shows that the percentage of dry years during MAM from moderate to extremely dry (SPI<-1) is less than that of wet years (SPI > 1) over all sub regions. The wet (dry) years during MAM under RCP8.5 scenarios account for about 13.3% (18.5%), 11.7% (15.0%), and 11.7% (12.7%) of the total duration over NEA, EEA, and SEA respectively. Similarly, the wet (dry) seasons under RCP4.5 accounts for about 16.7% (16.7%), 11.7% (18.3%) and 13.3% (18.3%) from the total number of seasons during the projection period (2021–2080) over NEA, EEA and SEA respectively (see Fig. 9a). These figures suggest that MAM is drier under RCP4.5 than RCP8.5 scenario. This is in agreement with (Muhati et al., 2018) who arrived at a similar conclusion over the northern part of Kenya. On the other hand, the fraction of wet dry seasons during short rains (SOND) under RCP4.5 is 16.7% (18.3%), 20.0% (18.3%) and 18.3% (15.0%) of the total wet months over NEA, EEA and SEA respectively (Fig. 9). Similarly, 15.0% (20.0%), 16.7% (11.7%) and 16.7% (16.7%) of the projection years are wet (dry) over NEA, EEA, and SEA under RCP8.5 respectively. This shows the

percentage of wet years is anticipated to be numerous compared to dry years over EEA under RCP4.5 and RCP8.5.

The percentage of normal years (1 > SPI > âˆ’1) during MAM, under the two scenarios is almost comparable to the percentages of normal rainfall months identified by CRU rainfall. However, the percentage of normal rainy months during SOND identified from CRU and HEM rainfalls is more than that identified from rainfalls under RCP4.5 and RCP8.5 scenarios. The overall wet and dry months of the historical period during MAM are comparable in contrast to the projection period where wet months exceed dry months (Fig. 9 and Fig. 3). Similarly, during SOND, the percentage of the normal rainy months under the two climate change scenarios is more (less) than that of CRU over NEA, EEA and SEA. On the other hand, the percentage of wet rainy months of the projected rainfalls is more (less) than that of CRU over NEA, EEA and SEA (see Fig. 9 and Fig. 3). This shows that more frequent wet and dry conditions in different parts of EA are expected during the projection period relative to the historical period.

Spatial distribution of percentage of wet (SPI $\geq$ 1) and dry (SPI $\leq$ -1) months of both seasons from 2021 to 2080 are given in Fig. 10. The fractions of wet months under both RCP4.5 and RCP8.5 are comparable over most of EA during MAM season (Fig. 10a-b). This is not the case during SOND in particular over Somalia, southeastern Kenya, South Sudan and adjoining areas in Uganda (Fig. 10c-d). Moreover, the percentage of dry rainy months over EA under the two scenarios during MAM and SOND exhibits significant differences (Fig. 10e-h). As already noted from the analysis of historical observations, it is worth comparing the proportion of wet and dry months in the projections as given in Fig. 10i-l. Dry conditions (red color) are expected to be more frequent than wet conditions (blue color) over most parts of EA under both scenarios during the two seasons (Fig. 10k-l). However, there are a few exceptions over southern Ethiopia and adjoining northwestern Somalia, central Kenya, western Tanzania and Uganda during MAM under RCP4.5 where the wet conditions are expected to be more frequent than dry events (Fig. 10i-j). Likewise, more frequent wet than dry conditions over northwestern and eastern Kenya during MAM under RCP8.5 (Fig. 10j), over central Uganda, southern South Sudan, southeastern Kenya, western Somalia during SOND under RCP4.5 (Fig. 9k) and over southern Ethiopia under RCP8.5 during SOND (Fig. 10l) are observed from ensemble mean of the projections of the models. More frequent occurrence of dry than wet conditions under both projections during MAM implies the continuation of more dry conditions observed during the historical period into the projection period (see Fig. 4i-j and Fig. 10i-j). In contrast, during SOND, more dry events are expected during projection relative to the historical observations (compare Fig. 4k-l and Fig. 10k-l) suggesting a possible shift in the frequency distribution of extreme events during SOND. On average, the wet (dry) seasons will account for about 16.1 %(16.2%) under RCP4.5 (Fig. 10a, e) scenarios and 16.0% (15.6%) under RCP8.5 scenarios (Fig. 10b, f) during MAM, and 16.6% (16.1%) under RCP4.5 (Fig. 10c, g) and 16.2% (15.9%) under RCP8.5 (Fig. 10d, h) during SOND respectively. The average number of normal seasons under RCP4.5 (RCP8.5) is also expected to account for about 67.8% (68.4%) during MAM and 67.3% (67.9%) during SOND respectively. The difference between the percentage of extreme events (Fig. 10i-l) revealed that the number of extreme wet events exceed that of extreme dry events under RCP4.5 during SOND and under RCP8.5 during both seasons.

3.2.4. Spatiotemporal variability of projected PCI

PCI under both projected scenarios in MAM and SOND over each sub region is given in Table 7. The monthly precipitation distribution in MAM is expected to be moderate (98.2%) and uniform (10.9%) over NEA, uniform (100%) over EEA and moderate (100%) over SEA under RCP4.5. Similarly, projected PCI under RCP8.5 shows that temporal rainfall distribution within MAM season is expected to be moderate (95%) over NEA, uniform (100%) over EEA and moderate (100%) over SEA. As a whole, EA is also expected to experience uniformly distributed rainfall temporarily as confirmed from uniform PCI values under both projected scenarios. In general, the ranges of PCI values in MAM under both projected scenarios are within the categories of moderate and uniform temporal rainfall distribution over NEA, uniform over EEA and moderate over SEA. Rainfall during boreal autumn season under RCP4.5 is expected to be moderately (95%) and irregularly (5%) distributed over NEA, uniformly (100%) over EEA, and moderately (100%) over SEA. Similarly, rainfall distribution within the months of SOND season under RCP8.5 is expected to be moderate (96.7%) over NEA, uniform (100%) over EEA, and moderate (100%) over SEA (see Table 7). As a result, precipitation concentration from both projections will not change relative to the historical period as represented by HEM and CRU over each sub region and the whole EA implying expected climate change under the two scenarios will not alter current precipitation heterogeneity.

Table 7
Number of years with uniform, moderate, irregular and strong irregular PCI values in boreal spring and autumn seasons.

Rainfall	PCI range	MAM				SOND			
		NEA	EEA	SEA	EA	NEA	EEA	SEA	EA
RCP4.5	$8.3 < PCI \leq 10$	6	60	0	60	3	60	0	60
	$10 < PCI \leq 15$	54	0	60	0	57	0	60	0
	$15 < PCI \leq 20$	0	0	0	0	0	0	0	0
RCP8.5	$8.3 < PCI \leq 10$	0	60	0	60	0	60	0	60
	$10 < PCI \leq 15$	57	0	60	0	58	0	60	0
	$15 < PCI \leq 20$	3	0	0	0	2	0	0	0

The projected PCI trend of both short and long rains under both scenarios is given in Table 8. Trend of PCI over EEA, SEA, and EA under RCP4.5 as well as trend of PCI over EEA and EA under RCP8.5 are positive in MAM. Similarly, PCI trend over EEA, SEA and EA under both RCP4.5 and RCP8.5 are positive in SOND. In contrast, NEA is expected to experience negative PCI trends during both seasons under the two scenarios. The identified sign of the projected trends under the two scenarios imply tendency towards more of irregular rainfall concentration in the future over EEA, SEA and the whole EA as compared to a shift towards more of uniform over NEA particularly during SOND.

Table 8
Projected PCI trend under RCP4.5 and RCP8.5 rainfalls from 2021 to 2080 per decade.

Sub region	MAM		SOND	
	RCP4.5	RCP8.5	RCP4.5	RCP8.5
NEA	-0.06	-0.13	-0.16	-0.21
EEA	0.03	0.01	0.03	0.01
SEA	0.14	-0.11	0.04	0.01
EA	0.02	0.01	0.01	0.01

In general, there is no appreciable PCI difference in both seasons in the historical and projection periods using spatial mean of rainfall over each sub region. However, it is important to investigate PCI maps for any change in long term mean of seasonal PCI relative to the historical PCI values. Map of PCI over EA under both scenarios in MAM and SOND is given in Fig. 11. Grid point long term mean PCI during MAM is expected to be uniform over central and northeastern Ethiopia, northern DRC, Uganda, southern part of South Sudan, western and southern Kenya, and northern and eastern Tanzania under both RCP4.5 and RP8.5. Moderate mean PCI is expected over South Sudan, Sudan Republic, western, southwestern, southern and southeastern Ethiopia, eastern Kenya, Somalia, southern DRC and most parts of Tanzania under both scenarios (Fig. 11a-b). On average, irregular PCI is expected over southern DRC and adjoining part of Tanzania under both scenarios. Mean uniform PCI pattern extending from west to east is expected over DRC, South Sudan, Uganda, and Kenya and adjoining part of Tanzania under both scenarios. This PCI pattern is also observed in CRU and HEM rainfalls from 1951 to 2005 (see Fig. 5a-b) except for the minor difference in southwest to northeast orientation of uniform PCI over southern Ethiopia. Southern DRC and southern Tanzania are expected to show irregular PCI values under both projections. Areal extent of moderate PCI is broader than that of uniform PCI which is also observed within the historical period. Grid point temporal means PCI during SOND is expected to be uniform over some areas in DRC, Uganda, and northern Tanzania and Kenya under both scenarios. Uniform PCI coverage is much smaller than moderate PCI coverage. Unlike MAM, irregular PCI is expected over Sudan Republic, northwestern Ethiopia and southern Tanzania during SOND (Fig. 11c-d). Overall, the projected mean PCI maps show that there is no shift in the mean PCI over EA as a whole relative to the historical period except for minor differences at some places.

4. Conclusions

The climatological seasonal average of HEM and CRU rainfalls exhibit similar type of dipole spatial pattern in both MAM and SOND consistent with past studies from observations. The agreement between HEM and CRU rainfalls in terms of reproducing the dipole spatial structure indicates the fidelity of the models used in the ensemble mean as confirmed in our previous studies. The same spatial patterns in seasonal averages of the projected rainfalls under RCP4.5 and RCP8.5 are noticed in the two seasons

implying the persistence of this spatial rainfall distribution into the projection period. This is expected from observation and also from robust models since the dipole structure over EA is primarily linked to the north-south migration of ITCZ location with seasons following the Earths revolution around the Sun. Projection values under both scenarios are expected to be wetter than historical period as revealed from comparison of spatial mean of CRU and HEM over EEA and SEA in SOND whereas the opposite is true over NEA in all months and over EEA and SEA from December to October. EA is also expected to experience wetter condition under RCP8.5 than RCP4.5 scenarios during short rains in contrast to long rains.

This seasonal difference under the two scenarios is also prevalent in the historical rainfalls of the two seasons. For example, the spatial mean of HEM and CRU rainfalls over the three sub regions (i.e. NEA, EEA and SEA) show wet trend in SOND and dry trend in MAM in agreement with several previous studies. Most parts of EA over northwestern and southeastern Ethiopia, Kenya, Tanzania and DRC in MAM and northwestern Ethiopia and adjoining parts of South Sudan, some parts of DRC and central parts of Kenya in SOND have shown dry trend in CRU rainfalls. HEM rainfalls over Ethiopia and DRC in MAM and over DRC and Tanzania in SOND have dry trend. The models tend to be wetter than the observations since HEM has exhibited wet trend than CRU over the region.

Projected rainfalls in SOND are expected to show more of wet trend over NEA from 2021 to 2080 but the opposite is expected over SEA and EEA. RCP4.5 is expected to show more of dry trend compared to RCP8.5 during the projected period. Projected rainfall during boreal spring season show wet trends over EEA and SEA but the opposite is true over NEA. The projected trend is opposite of HEM and CRU trends of historical period. CRU has more of wet anomalies compared to HEM relative to mean values from base period (i.e mean values from 1971 to 2000) during both rainy seasons. Anomalies of rainfall under both projected rainfalls are expected to be positive anomalies during boreal autumn season. On the other hand, projected rainfalls during boreal spring season are expected to show dry anomalies. Rainfall projected under RCP8.5 has more of wet anomalies compared with projected rainfalls under RCP4.5.

The proportion of wet events captured by CRU and HEM is comparable at most places over EA during MAM in contrast to significant difference during SOND implying the ensemble mean skill of the models in capturing extreme wet conditions is better during MAM than SOND. However, the ensemble mean skill of the models in reproducing extreme dry events from CRU during MAM and SOND over EA is relatively low as reflected by apparent difference between number of dry events in CRU and HEM. Most of EA has experienced more of dry events than wet events during MAM as captured by both CRU and HEM with the exceptions of a few isolated places with more wet events than dry events. CRU rainfall shows that wet events are more frequent than dry events over nearly half of EA during SOND. The wet events are as frequent as dry events over the other half of EA with the exceptions at a few isolated places in South Sudan and Tanzania where dry events dominate over wet events. The frequency of wet events under both RCP4.5 and RCP8.5 scenario projections during MAM season is comparable over most of EA. This is not the case during SOND at most places over EA. However, it is difficult to conclude whether this is attributed to scenario difference or to limited skills of the models during SOND as confirmed earlier from

comparison of historical observations and simulations. The same ambiguity arises regarding the difference in frequency of dry events over EA under the two scenarios during MAM and SOND. Dry events are expected to be more frequent than wet events over most parts of EA under both scenarios during both seasons. However, this conclusion suffers from uncertainty related to limited skill of the model during SOND.

MAM rainfall is uniformly distributed within the three months of the season over most parts of EA as confirmed by both CRU observations and HEM simulations. A few boarder areas in southwestern and northwestern EA exhibit moderate heterogeneity in MAM rainfall distributions. However, during SOND, rainfall exhibits strong heterogeneity as reflected in irregular distribution of CRU rainfall within the four months of the season over southern Tanzania, western Ethiopia and South Sudan. The rainfall distribution from HEM simulations exhibit nearly similar features over these areas. However, the amplified signals in PCI over these areas may also suffer from uncertainty arising from limited skills of the models in capturing rainfall variability over the region in general. There is also evidence of a shift from more uniform or moderate mean distribution in current climate to moderate or irregular mean distribution in the projection during MAM over southern EA mainly southern Tanzania and adjoining DRC. However, the observed and simulated moderate to irregular mean rainfall distribution of the historical period over western Ethiopia and Sudan during SOND is expected to shift towards more of uniform or moderate rainfall distribution during the projection periods whereas the moderate to irregular distribution over southern parts of SEA in the current climate is expected to shift towards more of uniform or moderate distribution under the projections. These changes might slightly also suffer from the uncertainty that arises from limited model skill during SOND in capturing observed PCI.

In summary, the HEM simulations are worth of considerations when investigating change in mean climate, frequency of extreme precipitations and precipitation heterogeneity during both historical and projections period. In contrast, the skill of the models used in the ensemble mean simulations in capturing both trends during the two dominant seasons of EA is still limited over much of EA. Therefore, the wetting trend depicted by HEM simulations during historical and a projection period is in clear contrast to observation particularly during MAM suggesting that the need for tuning the model through controlled process studies.

Declarations

Acknowledgements

The authors would like to acknowledge greatly World Climate Research Programme (WCRP) for access to precipitation data. The first author also would like to extend gratitude to Wollo University department of physics for sponsorship and support

Author Contributions

The first author retrieved historical and projected data, designed and wrote the analysis procedure, and produced the figures presented in this paper. The second author followed every step and provided valuable procedural steps for each figure, table and ideas. He has also reviewed the manuscript from the very beginning to this level. Both authors have equally contributed to the paper.

Competing financial interests

The authors declare no competing financial interests

Conflict of interest

The authors declare that they have no conflict of interest.

Data availability

Observed gridded precipitation is taken from Climate Research Unit (CRU: version 4.04) of East Angela University. Information on the data is available at http://badc.nerc.ac.uk/data/cru/â€. Model simulated data are taken from CMIP5 repository, which is downscaled in the framework of CORDEX.

Code availability

Shape file used for boundary delimitation is available at https://github.com/nvkelso/naturalearth-vector/blob/master/ 50m cultural/ne 50m. Mathematical equations given in the introduction part are also converted to simple codes, and can be available in any request.

Ethics approval and consent to participate

Not applicable

Consent for publication

Not applicable

References

1. Allan R, Soden B (2008) Atmospheric Warming and the Amplification of Precipitation Extremes. Sci (New York N Y) 321:1481–1484. https://doi.org/10.1126/science.1160787
2. Allen, Barros V, Broome J, Cramer W, Christ R, Church J, Clarke L, Dahe Q, Dasgupta P, Dubash N, Edenhofer O, Elgizouli I, Field C, Forster P, Friedlingstein P, Fuglestvedt J, Gomez-Echeverri L, Hallegatte S, Hegerl G (2014) & Urge-Vorsatz, D. *Climate Change 2014: Synthesis Report*
3. Anyah RO, Semazzi FHM (2007) *Variability of East African rainfall based on multiyear RegCM3 simulations*. *371*(September 2006), 357–371. https://doi.org/10.1002/joc
4. Arora VK, Scinocca JF, Boer GJ, Christian JR, Denman KL, Flato GM, Kharin VV, Lee WG, Merryfield WJ (2011) *Carbon emission limits required to satisfy future representative concentration pathways*

of greenhouse gases. *38*, 3–8. https://doi.org/10.1029/2010GL046270

5. Assamnew AD, Gizaw MT (2020) The performance of regional climate models driven by various general circulation models in reproducing observed rainfall over East Africa. *Theoretical and Applied Climatology(2020)*. https://doi.org/https://doi.org/10.1007/s00704-020-03357-3
6. Ayugi B, Tan G, Gnitou GT, Ojara M, Ongoma V (2019) Jo u rn al Pr. Atmos Res 104705. https://doi.org/10.1016/j.atmosres.2019.104705
7. Bahaga TK, Kucharski F, Tsidu GM (2015) *Assessment of prediction and predictability of short rains over equatorial East Africa using a multi-model ensemble*. *Jury 2002*. https://doi.org/10.1007/s00704-014-1370-1
8. Bobadoye A, Ogara W, Ouma G, Onono J (2016) Assessing Climate Change Adaptation Strategies among Rural Maasai pastoralist in Kenya. Am J Rural Dev 4(6):120–128. https://doi.org/10.12691/ajrd-4-6-1
9. Brunswick N, Sciences A, Carolina N, Sciences A, Carolina N (2006) *Simulated Physical Mechanisms Associated with Climate Variability over Lake Victoria Basin in East Africa*. 3588–3609
10. Cattani E, Merino A, Guijarro JA, Levizzani V (2018) East Africa Rainfall trends and variability 1983–2015 using three long-term satellite products. Remote Sens 10(6):1–26. https://doi.org/10.3390/rs10060931
11. Church J, Clark P, Cazenave A, Gregory J, Jevrejeva S, Levermann A, Merrifield M, Milne G, Nerem R, Nunn P, Payne A, Pfeffer W, Stammer D, Alakkat U (2013) Climate Change 2013: The Physical Science Basis. Contribution of Working Group I to the Fifth Assessment Report of the Intergovernmental Panel on Climate Change.Sea Level Change,1138–1191
12. Courtier P, Thépaut J-NJ-N, Hollingsworth A, Martens B, Schumacher DL, Wouters H, Muñoz-Sabater J, Verhoest NEC, Miralles DG, Gebremicael T, Mohamed Y, van der Zaag P, Berhe A, Haile G, Hagos E, Hagos M, Manatsa D, Chingombe W, Matarira CH, Hollingsworth A (2020) Numerical investigation on the power of parametric and nonparametric tests for trend detection in annual maximum series. Int J Climatol 24(1):124168. https://doi.org/10.5194/hess-24-473-2020
13. De Luis M, González-Hidalgo JC, Brunetti M, Longares LA (2011) Precipitation concentration changes in Spain 1946–2005. Nat Hazards Earth Syst Sci 11(5):1259–1265. https://doi.org/10.5194/nhess-11-1259-2011
14. Diro GT, Tompkins AM, Bi X (2012) *Dynamical downscaling of ECMWF Ensemble seasonal forecasts over East Africa with RegCM3*. *117*(October 2011), 1–20. https://doi.org/10.1029/2011JD016997
15. Elizalde A, Haensler A, Hagemann S, Jacob D, Kumar P, Podzun R, Remedio A, Saeed F, Teichmann C, Wilhelm C (2010) Validation of the regional climate model REMO over several CORDEX regions throughout the globe. Geophys Res Abstracts 12:11951
16. Evans JP (2011) CORDEX - An international climate downscaling initiative. *MODSIM 2011–19th International Congress on Modelling and Simulation - Sustaining Our Future: Understanding and Living with Uncertainty*, *December*, 2705–2711. https://doi.org/10.36334/modsim.2011.f5.evans

17. Gebrechorkos SH, Hülsmann S, Bernhofer C (2018) Evaluation of multiple climate data sources for managing environmental resources in East Africa. Hydrol Earth Syst Sci 22(8):4547–4564. https://doi.org/10.5194/hess-22-4547-2018
18. Giorgetta MA, Jungclaus J, Reick CH, Legutke S, Bo M, Brovkin V, Crueger T, Esch M, Fieg K, Glushak K, Gayler V, Haak H, Hollweg H, Ilyina T, Kinne S, Kornblueh L, Matei D, Mauritsen T, Mikolajewicz U, Claussen M (2013) *Climate and carbon cycle changes from 1850 to 2100 in MPI-ESM simulations for the Coupled Model Intercomparison Project phase 5*. *5*, 572–597. https://doi.org/10.1002/jame.20038
19. Gutowski, W., Giorgi, F., Timbal, B., Frigon, A., Jacob, D., Kang, H.-S., Raghavan,K., Lee, B., Lennard, C., Nikulin, G., O'Rourke, E., Michel, R., Solman,S., Stephenson, T., & Tangang, F. (2016). WCRP COordinated Regional Downscaling EXperiment(CORDEX): a diagnostic MIP for CMIP6. *Geoscientific Model Development*, *9*, 4087–4095. https://doi.org/10.5194/gmd-9-4087-2016
20. Jacob D, Elizalde A, Haensler A, Hagemann S, Kumar P, Podzun R, Rechid D, Remedio AR, Saeed F, Sieck K, Teichmann C, Wilhelm C (2012) *Assessing the Transferability of the Regional Climate Model*. 181–199. https://doi.org/10.3390/atmos3010181
21. Jones CG, Samuelsson P, Kjellström E (2011) Regional climate modelling at the Rossby Centre. Tellus Ser A: Dynamic Meteorol Oceanogr 63(1):1–3. https://doi.org/10.1111/j.1600-0870.2010.00491.x
22. Kharin VV, Zwiers FW, Zhang XB, Hegerl GC (2007) Changes in temperature and precipitation extremes in the IPCC ensemble of global coupled model simulations. J Clim 20(8):1419–1444. https://doi.org/10.1175/JCLI4066.1
23. Knutti R, Sedlá˘ J (2012) Robustness and uncertainties in the new CMIP5 climate model projections. Nat Clim Change 3(4):369–373. https://doi.org/10.1038/nclimate1716
24. Krishnan R, Singh M, Vellore R, Mujumdar M (2019) Progress and prospects in weather and climate modelling.Physics News,1–8
25. Liebmann B, Hoerling MP, Funk C, Bladé I, Dole RM, Allured D, Quan X, Pegion P, Eischeid JK (2014) Understanding recent eastern Horn of Africa rainfall variability and change. J Clim 27(23):8630–8645. https://doi.org/10.1175/JCLI-D-13-00714.1
26. Lyon B, Dewitt DG (2012) A recent and abrupt decline in the East African long rains. Geophys Res Lett 39(2):1–5. https://doi.org/10.1029/2011GL050337
27. Lyon B, Vigaud N (2017a) *Unraveling East Africa's Climate Paradox: Patterns and Mechanisms* (pp. 265–281). https://doi.org/10.1002/9781119068020.ch16
28. Lyon B, Vigaud N (2017b) *Unraveling East Africa ' s Climate Paradox*. 265–281
29. Measham TG, Lumbasi JA (2013) *Success Factors for Community-Based Natural Resource Management (CBNRM): Lessons from Kenya and Australia*. https://doi.org/10.1007/s00267-013-0114-9
30. Mitchell TD, Jones PD (2005) An improved method of constructing a database of monthly climate observations and associated high-resolution grids. Int J Climatol 25(6):693–712.

https://doi.org/10.1002/joc.1181

31. Mostafa AN, Wheida A, El M, Adel M, El L, Siour G, Coman A, Borbon A, Wahab A, Omar M, Saad-hussein A, Alfaro SC, Syst LI (2019) Past (1950–2017) and future (2100) temperature and precipitation trends in Egypt. Weather and Climate Extremes 100225. https://doi.org/10.1016/j.wace.2019.100225
32. Muhati GL, Olago D, Olaka L (2018) Past and projected rainfall and temperature trends in a sub-humid Montane Forest in Northern Kenya based on the CMIP5 model ensemble. Global Ecol Conserv 16:e00469. https://doi.org/10.1016/j.gecco.2018.e00469
33. Ngoma H, Wen W, Ojara M, Ayugi B (2021) *Assessing Current and Future Spatiotemporal Precipitation Variability and Trends Over Uganda, East Africa Based on Chirps and Regional Climate Models Datasets*. https://doi.org/10.20944/preprints202101.0037.v1
34. Nguvava M, Abiodun BJ, Otieno F (2019) Projecting drought characteristics over East African basins at speci fi c global warming levels. *Atmospheric Research*, *228*(November 2018), 41–54. https://doi.org/10.1016/j.atmosres.2019.05.008
35. Nicholson SE (2017) *Climate and Climatic Variability of Rainfall over Eastern Africa*. https://doi.org/10.1002/2016RG000544
36. Ntwali D, Ogwang BA, Ongoma V (2016) The Impacts of Topography on Spatial and Temporal Rainfall Distribution over Rwanda Based on WRF Model. Atmospheric and Climate Sciences 06(02):145–157. https://doi.org/10.4236/acs.2016.62013
37. Oliver JE (1980) Monthly precipitation distribution: A comparative index. Prof Geogr 32(3):300–309. https://doi.org/10.1111/j.0033-0124.1980.00300.x
38. Omondi PAo, Awange JL, Forootan E, Ogallo LA, Barakiza R, Girmaw GB, Fesseha I, Kululetera V, Kilembe C, Mbati MM, Kilavi M, King'uyu SM, Omeny PA, Njogu A, Badr EM, Musa TA, Muchiri P, Bamanya D, Komutunga E (2014) Changes in temperature and precipitation extremes over the Greater Horn of Africa region from 1961 to 2010. Int J Climatol 34(4):1262–1277. https://doi.org/10.1002/joc.3763
39. Ongoma V, Chen H, Gao C (2019) Evaluation of CMIP5 20th century rainfall simulation over the Equatorial East Africa. *Theoretical and Applied Climatology*, *On-line*. https://doi.org/10.1007/s00704-018-2392-x
40. Ongoma V, Chena H, Gaoa C (2018) Projected changes in mean rainfall and temperature over east Africa based on CMIP5 models. Int J Climatol 38(3):1375–1392. https://doi.org/10.1002/joc.5252
41. Overview A, Design E (2012) *An Overview of CMIP5 and*. *3*(april), 485–498. https://doi.org/10.1175/BAMS-D-11-00094.1
42. Samuelsson P, Jones C, WillÃ©n U, Ullerstig A, Gollvik S, Hansson U, Jansson C, KjellstrÃ¶m E, Nikulin G, Wyser K (2011) The Rossby Centre Regional Climate model RCA3: model description and performance. Tellus A 4–23. https://doi.org/10.3402/tellusa.v63i1.15770
43. Segele ZT, Leslie M, Lamb PJ (2009) *Evaluation and adaptation of a regional climate model for the Horn of Africa: rainfall climatology and interannual variability*. *65*(April 2008), 47–65.

https://doi.org/10.1002/joc

44. Sen PK (1968) Estimates of the Regression Coefficient Based on Kendall's Tau. J Am Stat Assoc 63(324):1379–1389. https://doi.org/10.1080/01621459.1968.10480934
45. Shiferaw A (2018) *Precipitation Extremes in Dynamically Downscaled Climate Scenarios over the Greater Horn of Africa*. 1–28. https://doi.org/10.3390/atmos9030112
46. Stiebert S, Murphy D, Dion J, Iisd M, Sawyer D (2012) *Kenya ' s Climate Change Action Plan: Mitigation. Chapter 1 : Methods, Key Findings and Priority Actions*. *August*, 22–29
47. Taylor K, Ronald S, Meehl G (2011) An overview of CMIP5 and the Experiment Design. Bull Am Meteorol Soc 93:485–498. https://doi.org/10.1175/BAMS-D-11-00094.1
48. Wainwright CM, Marsham JH, Keane RJ, Rowell DP, Finney DL, Black E, Allan RP (2019) 'Eastern African Paradox' rainfall decline due to shorter not less intense Long Rains. Npj Clim Atmospheric Sci 2(1):1–9. https://doi.org/10.1038/s41612-019-0091-7
49. Wang Y, Shilenje ZW, Sagero PO, Nyongesa AM, Banda N (2017) Rainfall variability and meteorological drought in the horn of Africa. Mausam 68(3):463–474. https://doi.org/10.54302/mausam.v68i3.678
50. Watanabe M, Suzuki T, O'ishi R, Komuro Y, Watanabe S, Emori S, Takemura T, Chikira M, Ogura T, Sekiguchi M, Takata K, Yamazaki D, Yokohata T, Nozawa T, Hasumi H, Tatebe H, Kimoto M (2010) Improved Climate Simulation by MIROC5: Mean States, Variability, and Climate Sensitivity. J Clim 23:6312–6335. https://doi.org/10.1175/2010JCLI3679.1
51. Williams AP, Funk C (2011) *A westward extension of the warm pool leads to a westward extension of the Walker circulation, drying eastern Africa*. *July 2010*, 2417–2435. https://doi.org/10.1007/s00382-010-0984-y
52. Woldemeskel FM, Sharma A, Sivakumar B, Mehrotra R (2015) J Geophys Research: Atmos 3–17. https://doi.org/10.1002/2015JD023719.Received
53. Wu M, Nikulin G, Kjellström E, Belušić D, Jones C, Lindstedt D (2020) The impact of regional climate model formulation and resolution on simulated precipitation in Africa. Earth Sys Dyn 11(2):377–394. https://doi.org/10.5194/esd-11-377-2020
54. Yang W, Seager R, Cane MA, Lyon B (2014) The East African long rains in observations and models. J Clim 27(19):7185–7202. https://doi.org/10.1175/JCLI-D-13-00447.1
55. Yang W, Seager R, Cane MA, Lyon B (2015) The annual cycle of East African precipitation. J Clim 28(6):2385–2404. https://doi.org/10.1175/JCLI-D-14-00484.1
56. Yisehak B, Shiferaw H, Abrha H, Gebremedhin A, Hagos H, Adhana K, Bezabh T (2021) Spatio-temporal characteristics of meteorological drought under changing climate in semi-arid region of northern Ethiopia. Environ Syst Res 10(1). https://doi.org/10.1186/s40068-021-00226-4

Figures

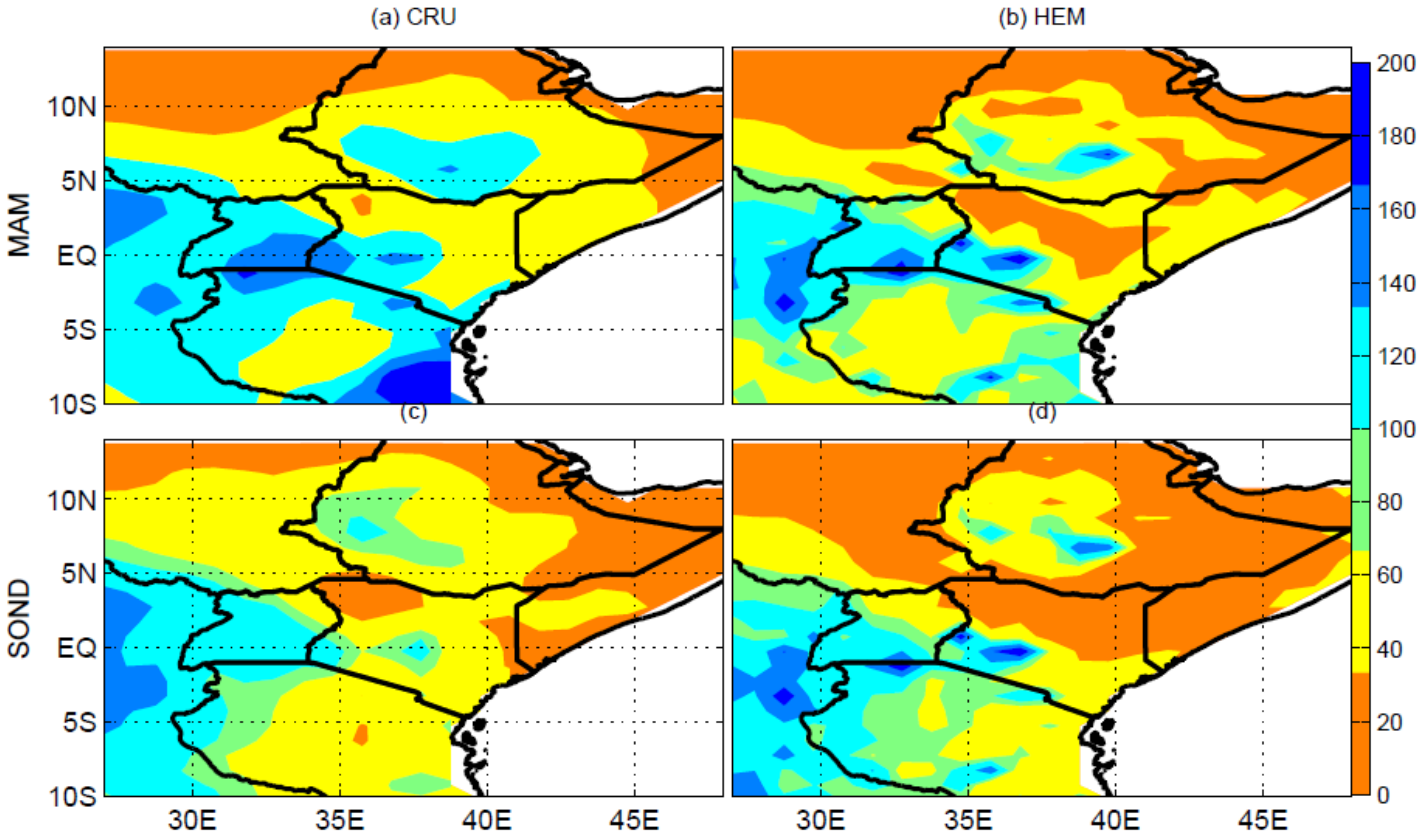

Figure 1

Spatial distribution of mean rainfalls over EA (mm/month) from CRU (a, c) and HEM (b, d) from 1951 to 2005

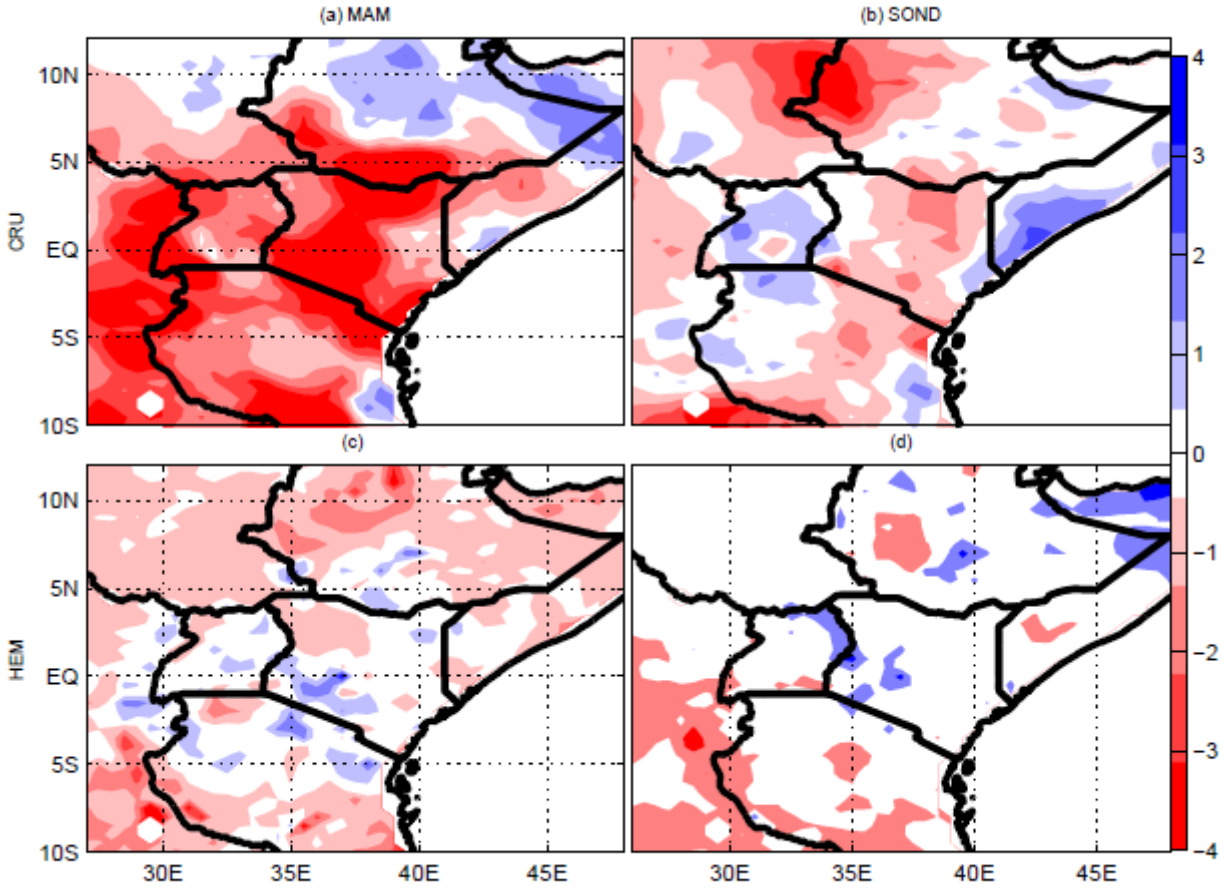

Figure 2

Seasonal rainfall trend (mm/decade) of CRU and HEM at each grid point from 1951 to 2005. The shaded in blue (red) colors represent wet (dry) trend respectively

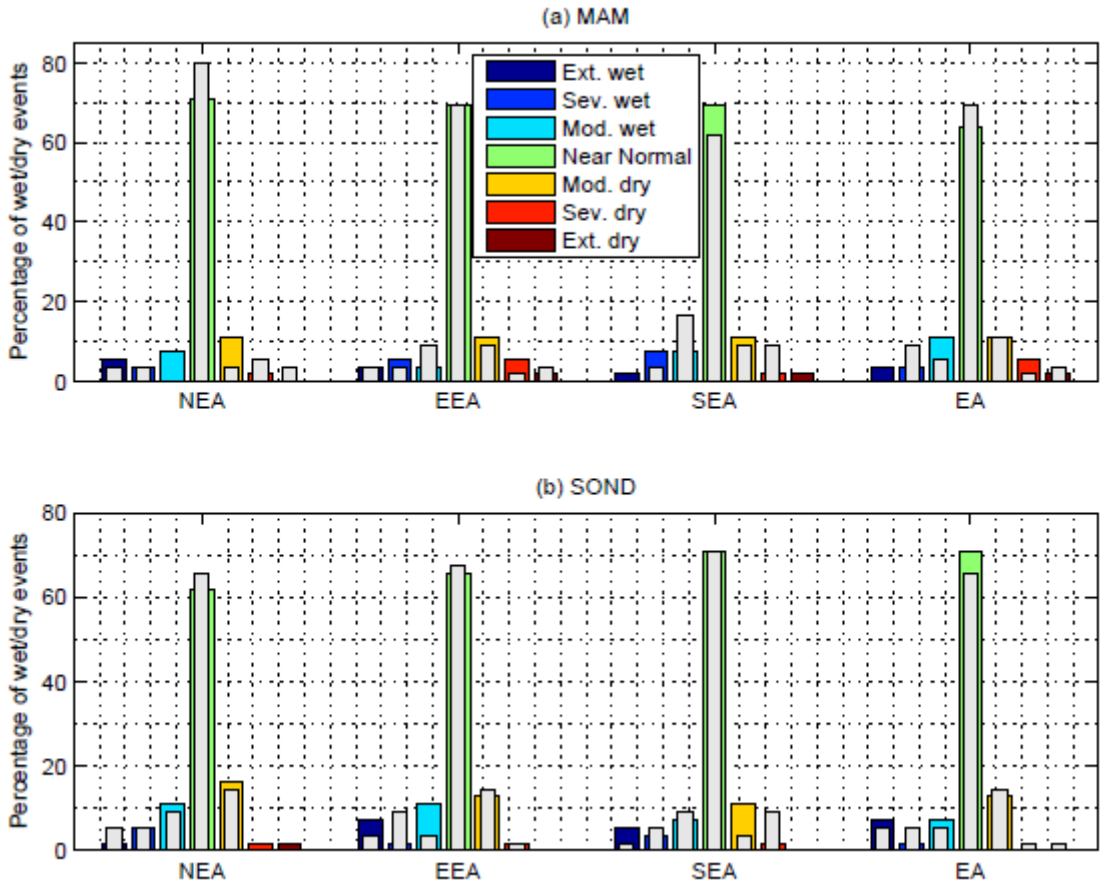

Figure 3

Percentage of wet and dry events for CRU (colored bars) and HEM (white bar) from 1951 to 2005.

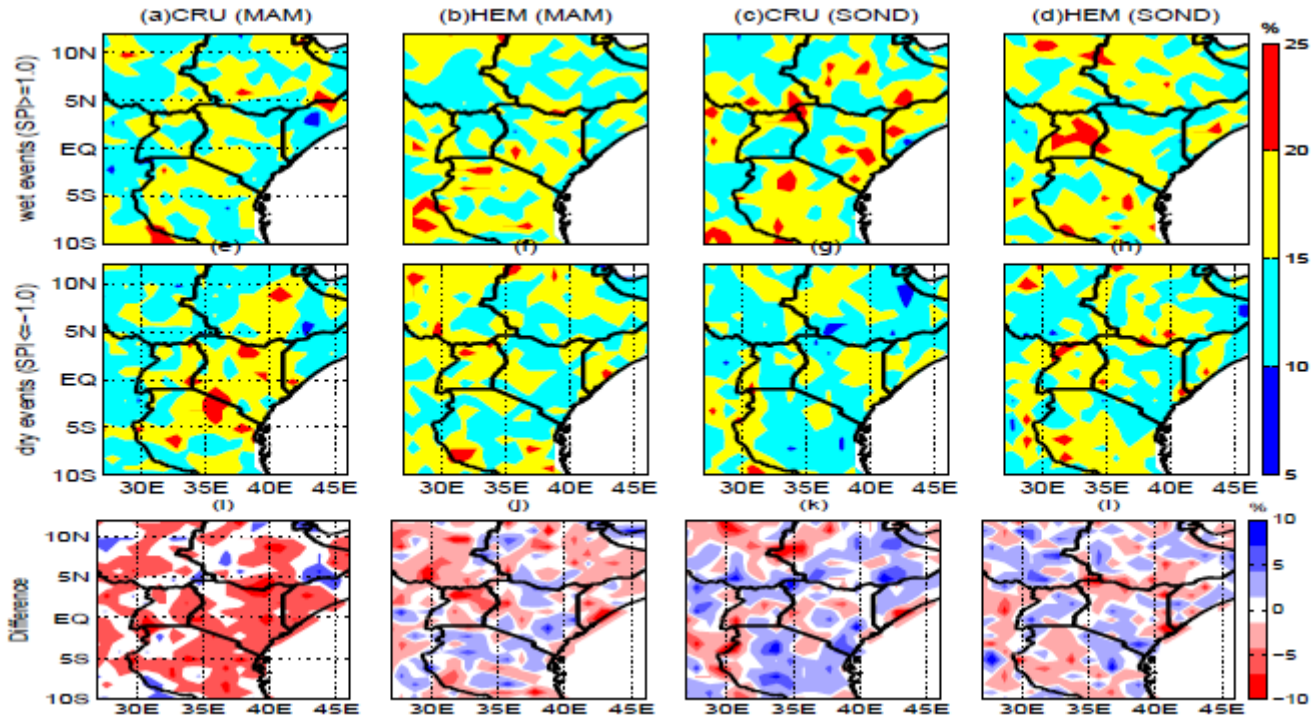

Figure 4

Percentage of wet events (a-d)(SPI ≥ 1), dry events (e-h)(SPI ≤ -1) and difference between wet events (first row) and dry events (second row) (i-l) during MAM (a, b, e, f, ,l, j) and SOND (c, d, g, h, k, l) from 1951 to 2005.

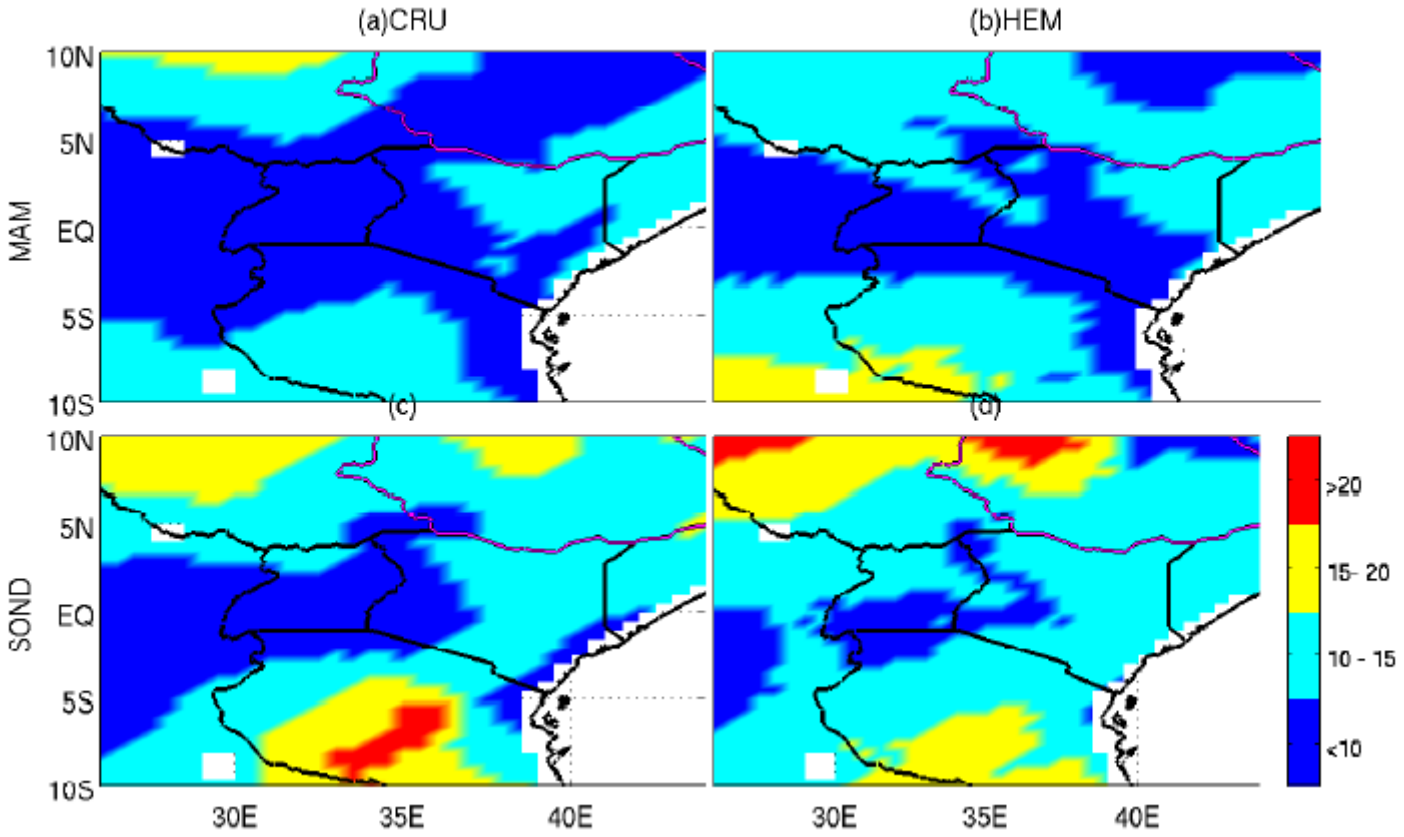

Figure 5

Grid point PCI distribution for long and short rains from 1951 to 2005 for HEM and CRU in MAM (a-b) and SOND (c-d).

Figure 6

The annual mean cycle of projected scenarios (2021 to 2080), HEM and CRU (1951 to 2005).

Figure 7

Spatial distribution of mean scenarios rainfalls over EA (mm/month) from RCP4.5 (a, c) and RCP8.5 (b, d) from 2021 to 2080.

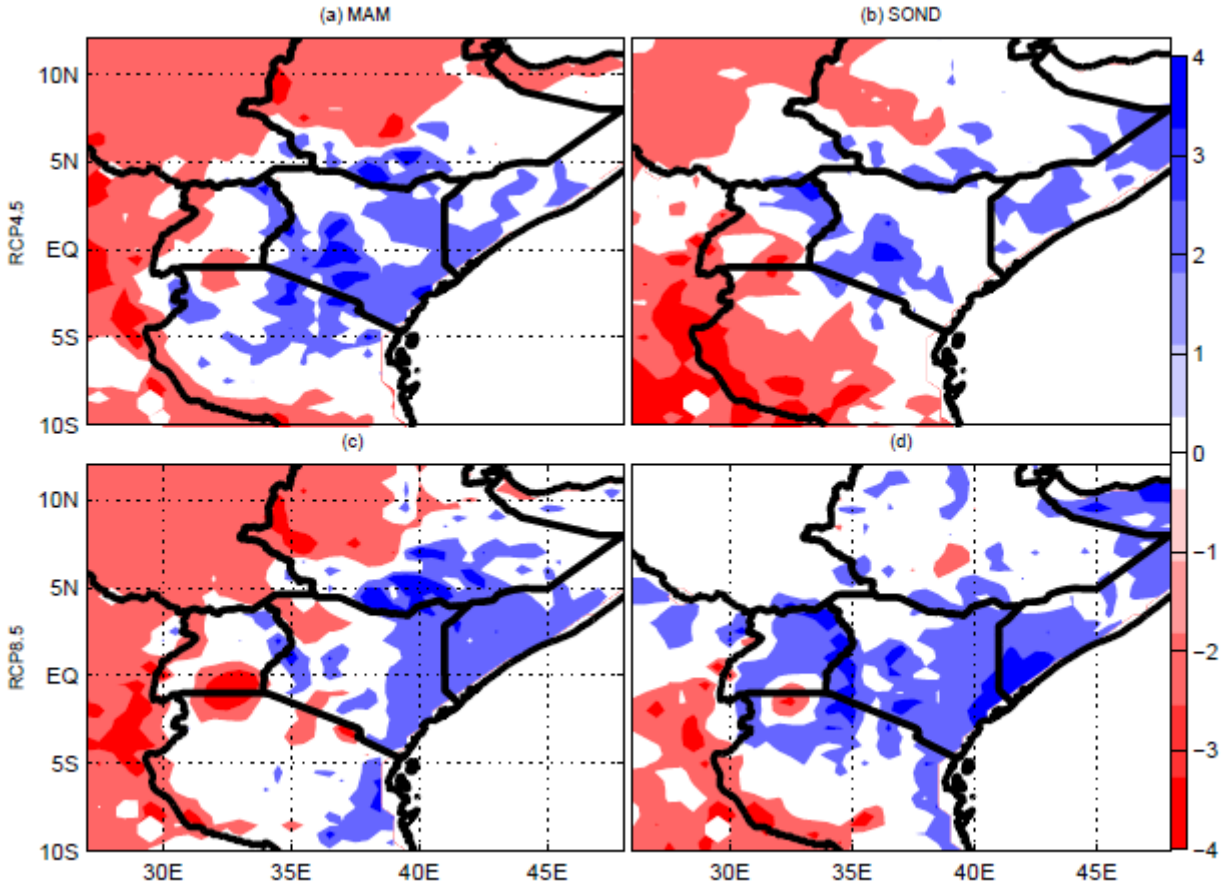

Figure 8

Seasonal rainfall trend (mm/decade) at each grid point over EA from 2021 to 2080

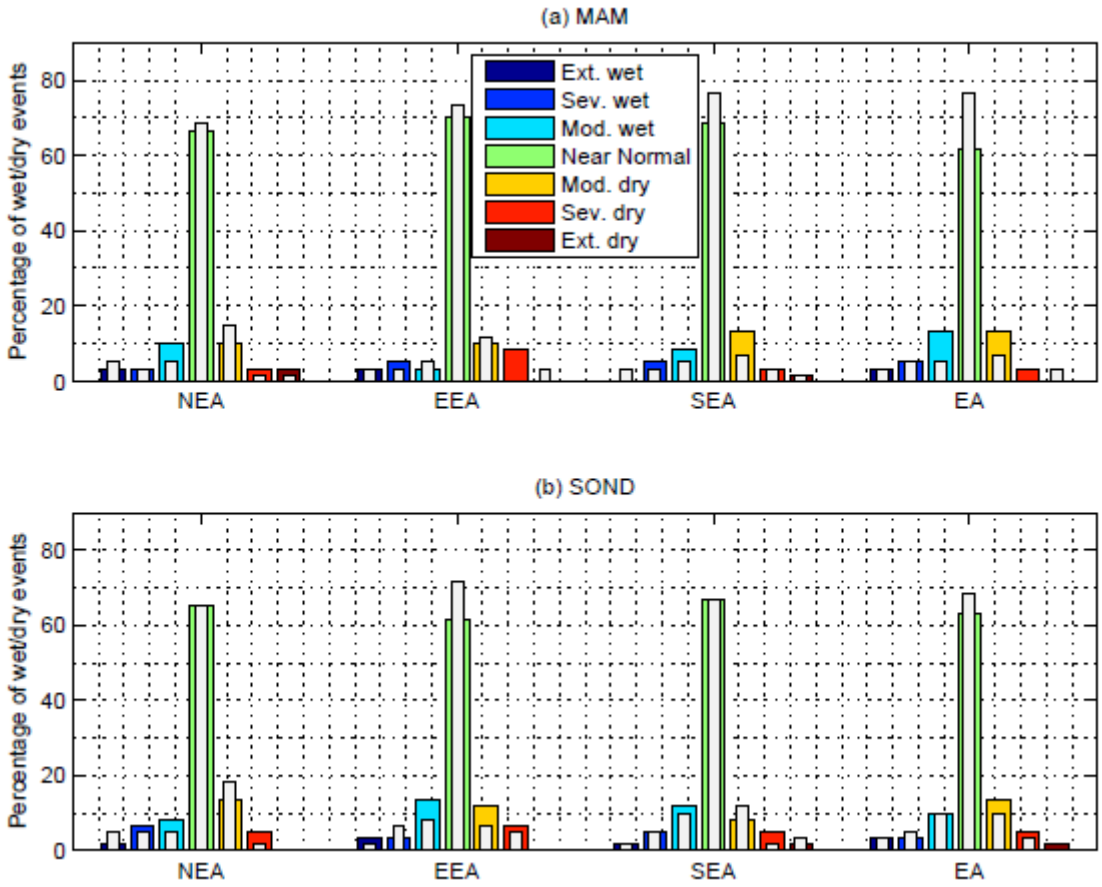

Figure 9

Percentage of wet and dry events of rainfalls projected under RCP4.5 (colored bars) and RCP8.5 (white bar) from 2021 to 2080.

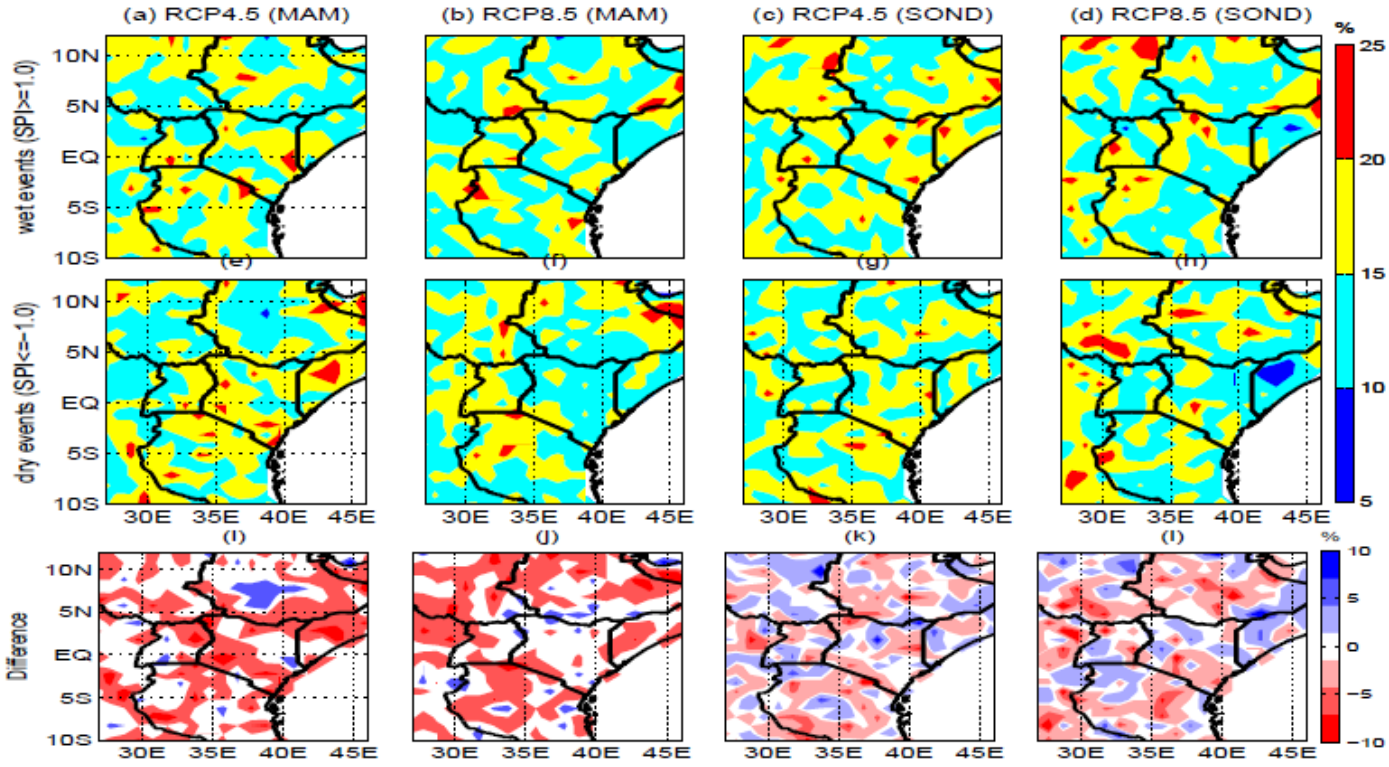

Figure 10

Percentage of wet events (SPI ≥1) (a-d), dry events (e-h) and difference between wet and dry events (SPI ≤ -1) (i-l) in MAM (a, b, e,f,i, j) and SOND (c, d, g, h, k, l) from 2021 to 2080.

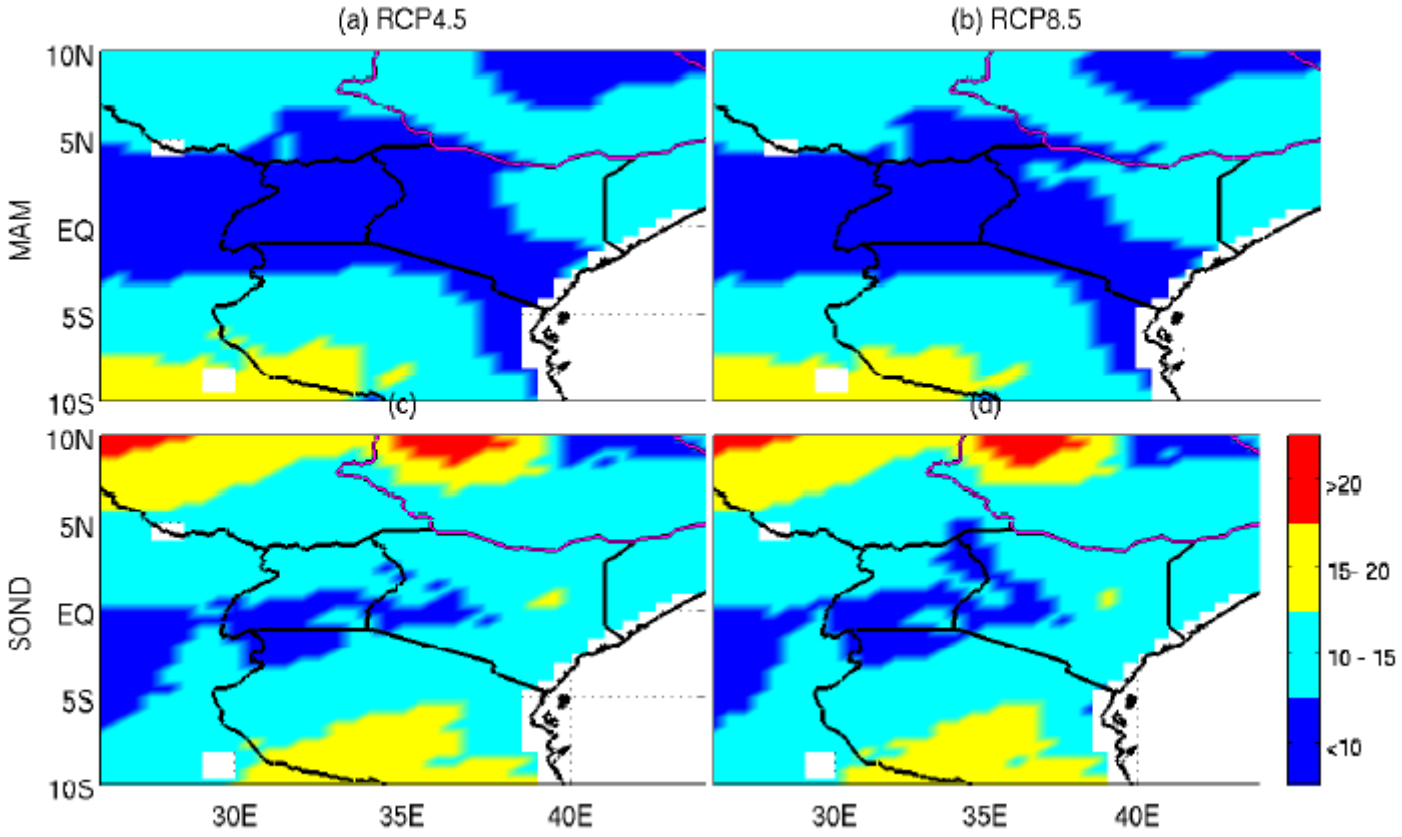

Figure 11

PCI distribution during MAM and SOND under RCP4.5 (a, c) and RCP8.5 (b, d) from 2021 to 2080.